Complete set of proton excitations in ^{119}Cs

K. K. Zheng,[1,2] C. M. Petrache,[1] Z. H. Zhang,[3] A. Astier,[1] B. F. Lv,[1,*] P. T. Greenlees,[4] T. Grahn,[4] R. Julin,[4] S. Juutinen,[4] M. Luoma,[4] J. Ojala,[4] J. Pakarinen,[4] J. Partanen,[4,†] P. Rahkila,[4] P. Ruotsalainen,[4] M. Sandzelius,[4] J. Sarén,[4] H. Tann,[4,5] J. Uusitalo,[4] G. Zimba,[4] B. Cederwall,[6] Ö. Aktas,[6] A. Ertoprak,[6] W. Zhang,[6] S. Guo,[2,7] M. L. Liu,[2,7] X. H. Zhou,[2,7] I. Kuti,[8] B. M. Nyakó,[8] D. Sohler,[8] J. Timár,[8] C. Andreoiu,[9] M. Doncel,[5] D. T. Joss,[5] and R. D. Page[5]

[1] *Université Paris-Saclay, CNRS/IN2P3, IJCLab, 91405 Orsay, France*
[2] *Key Laboratory of High Precision Nuclear Spectroscopy and Center for Nuclear Matter Science, Institute of Modern Physics, Chinese Academy of Sciences, Lanzhou 730000, People's Republic of China*
[3] *Mathematics and Physics Department, North China Electric Power University, Beijing 102206, China*
[4] *University of Jyväskylä, Department of Physics, P.O. Box 35, FI-40014, University of Jyväskylä, Finland*
[5] *Oliver Lodge Laboratory, Department of Physics, University of Liverpool, Liverpool L69 7ZE, United Kingdom*
[6] *KTH Department of Physics,S-10691 Stockholm, Sweden*
[7] *School of Nuclear Science and Technology, University of Chinese Academy of Science, Beijing 100049, People's Republic of China*
[8] *Institute for Nuclear Research (Atomki-ELKH), 4001 Debrecen, Hungary*
[9] *Department of Chemistry, Simon Fraser University, Burnaby, BC V5A 1S6, Canada*

(Dated:)

The very neutron-deficient strongly-deformed ^{119}Cs nucleus has been studied using the ^{58}Ni(^{64}Zn,3p) reaction and the JUROGAM 3 gamma-ray detector array coupled to the MARA recoil-mass separator setup. The excitation energies of all observed bands have been determined, spins and parities have been firmly assigned to most of the observed states. The previously known and the newly identified rotational bands have been extended to very high spin and excitation energy. The configurations of the observed bands are discussed using the particle number conserving cranked shell model. The present study establishes the largest set of rotational bands observed in the proton-rich $A \approx 120$ mass region.

PACS numbers: 21.10.Re, 21.60.Ev, 23.20.Lv, 27.60.+j

I. INTRODUCTION

The recent spectroscopic studies of cesium nuclei have been focused on chirality, which was observed in a long sequence of odd-odd nuclei from ^{122}Cs to ^{132}Cs [1]. The odd-even Cs nuclei have been the object of investigations devoted to the evolution of the collective properties far from stability [2–12]. However, the study of the lightest Cs nuclei is confronted with the increasing difficulty to populate high-spin states using fusion-evaporation reactions, due to the limited choice of projectile-target combinations and the small cross-sections for neutron evaporation close to the proton drip-line. The existing experimental information on high-spin states in very proton-rich nuclei is therefore increasingly scarce towards the proton-drip line. The lightest cesium nucleus with a rich band structure is ^{120}Cs [8]. In the other proton-rich Cs nuclei only one to three rotational bands are known, often without interconnecting transitions and unknown excitation energies. This prohibits a detailed comparison between theoretical calculations employing different interactions and experimental data, from which a fine tuning of the interactions used to describe very exotic nuclei can be done. Fortunately, the magnetic moments and spectroscopic quadrupole moments have been measured for long-lived isomers close to the ground states of an extended range of Cs nuclei, from ^{118}Cs to ^{145}Cs [13], which allowed to firmly assign spins and parities, and to experimentally determine their deformation. However, the interpretation of the observed band structures was often based on calculated deformations, which are significantly smaller than the measured ones. This induced in some cases difficulties to consistently assign configurations and to reproduce the crossing frequencies of the observed backbendings.

Very recently, new experimental results have been reported from the same high-statistics experiment from which the present results were obtained. The known bands have been extended at very high spin, and several new rotational bands have been identified: two positive-parity bands which decay to the known $\pi[404]9/2^+$ strongly-coupled band [14], and two positive-parity and one negative-parity bands built on prolate and oblate shapes, respectively [15]. These results revealed two exotic features of the band structure of ^{119}Cs: *i*) the existence of a new type of chiral bands which involve only

* Present address: Key Laboratory of High Precision Nuclear Spectroscopy and Center for Nuclear Matter Science, Institute of Modern Physics, Chinese Academy of Sciences, Lanzhou 730000, People's Republic of China
† Deceased

protons, one in the strongly-coupled $\pi[404]9/2^+$ orbital and two in $\pi h_{11/2}$ orbitals (Bands 8, 9, 10) [14]; *ii*) the existence of coexisting oblate and prolate shapes close to the ground state, which give rise to rotational bands with completely different behavior, one decoupled built on the $\pi[541]3/2^-$ orbital (Band 1) and one strongly coupled built on the $\pi[505]11/2^-$ orbital (Band 3) [15]. This two results represent discoveries of new phenomena, that is chirality with only protons in the back-bending regime and a new region of oblate-prolate shape coexistence in strongly-deformed nuclei at the proton-drip line.

The present work reports new results in ^{119}Cs, one of the less known Cs nuclei before the present experiment (only two floating bands were known [7]). A new ground state with spin-parity $3/2^+$ is established, seven cascades of $E2$ transitions grouped in five bands (Bands γ, 2, 4', 5' and 7), one band composed of $M1/E2$ and crossover $E2$ transitions (Band 6), and three other states which decay to Bands 1, 2 and 5. The relative energies of all bands are fixed by many interconnecting transitions. The spins and parities of most observed bands are determined based on measured angular correlation ratios and polarization asymmetries. The new Bands 2, 4' and 7 are observed up to very high spins of 83/2, 85/2 and 81/2, respectively.

The configurations of the observed bands are assigned based on particle number conserving cranked shell model (PNC-CSM) calculations [16, 17], leading to a coherent description of the observed rotational bands, and demonstrating the adequacy of the PNC-CSM model for the description of rotational bands in well deformed nuclei with nearly axial shapes.

II. EXPERIMENTAL DETAILS AND RESULTS

A. Experimental details

The ^{119}Cs nucleus has been investigated using the ^{58}Ni(^{64}Zn,3p) fusion-evaporation reaction with a beam energy of 255 MeV, and the JUROGAM 3 [18] plus MARA [19] setup at the Accelerator Laboratory of the University of Jyväskylä, Finland. A self-supporting enriched ^{58}Ni foil of 0.75 mg/cm^2 thickness was bombarded with a ^{64}Zn beam delivered by the K130 cyclotron. The fusion-evaporation residues were separated as a function of A/q and identified using the in-flight double-focusing recoil mass separator MARA [20]. At the focal plane a double-mass slit system was used to allow only two charge states of a given mass to be transported into the implantation detector. MARA is a mass separator but it cannot resolve isobars or overlapping evaporation channels involving α-particle evaporation due to the A/q ambiguity. A position-sensitive Multi-Wire-Proportional Counter (MWPC) is used at the focal plane to obtain A/q spectra. It comprises three wire planes: x-plane, cathode, and y-plane. The wire planes are realized with 20 μm thick gold-plated tungsten wires with 1 mm spacing. The final position is obtained using 2 ns delay lines between wires and by measuring the delays in the signals between the two ends of the wire planes. The implantation detector, placed 40 cm behind the MWPC, is a 300 μm thick Double-Sided-Silicon-strip Detector (DSSD) with a 0.67 mm strip width. The detector is 128 mm wide and 48 mm high, comprising 192 strips (x-plane) and 72 strips (y-plane) leading to a total of 13824 pixels. Behind the DSSD a second layer of silicon detectors (500 μm thick) is used for punch through events. The Time-of Flight (ToF) between the MWPC and DSSD is recorded. The ToF and the recoil energy deposited in the DSSD were used to distinguish between fusion recoils and scattered beam. Five clover germanium detectors surrounding the MARA focal-plane detection system were used to detect γ-rays emitted by long-lived isomers and daughters of the β-decay of the implanted recoils. All detector signals were recorded by the triggerless Total Data Readout (TDR) data acquisition system, and time stamped by a global 100 MHz clock which allowed to establish both temporal and spatial correlations between recoils and events obtained with the rest of the focal plane and JUROGAM 3 arrays [19, 21].

Prompt γ-rays were detected at the target position using the JUROGAM 3 germanium detector array consisting of 24 Euroball clover [22] and 15 Eurogam Phase I-type [23] escape-suppressed detectors, with an efficiency of $\approx 6\%$ at 1.3 MeV. The clover detectors were arranged symmetrically relative to the direction perpendicular to the beam (twelve at 75.5° and twelve at 104.5°), while the Phase I detectors were placed at backward angles with respect to the beam direction (five at 157.6° and ten at 133.6°).

The data were sorted using the GRAIN code [24]. In a first step the newly identified bands were assigned to ^{119}Cs using recoil-gated prompt coincidences and the presence of X-rays in the spectra. Following this identification, the analysis of the higher statistics prompt $\gamma\gamma\gamma$ coincidences without recoil gating enabled to construct a comprehensive level scheme, with a rich tapestry of band structures interconnected by a multitude of transitions. Fully symmetrized, three-dimensional (E_γ-E_γ-E_γ) matrices were analyzed using the RADWARE [25, 26] package. A total of 4×10^{10} prompt γ-ray coincidence events with fold ≥ 3 were collected.

The multipolarities of the γ-rays were extracted using the Directional Correlation from Oriented states (DCO) ratios (R_{DCO}) and two-point Angular Correlation (anisotropy) ratios R_{ac} [27, 28]. The R_{ac} values were extracted from γ-γ matrices, which were formed by sorting prompt coincidence events with (133.6° and 157.6°) versus (all angles) and (75.5° and 104.5°) versus (all angles) combinations, by setting the same energy gates on the (all angles) projection spectrum in both matrices, and projecting on the other axis. Then, the R_{ac} ratios were calculated using the extracted intensities of the γ-rays of interest (I_γ) from these spectra, normalized by the different efficiencies of the two sets of detectors, using the formula $R_{ac} = I_\gamma(133.6°{+}157.6°)/I_\gamma(75.5°{+}104.5°)$. The

typical values for stretched dipole and quadrupole transitions are around 0.8 and 1.4, respectively. The R_{DCO} values were also extracted from a γ-γ matrix, constructed by sorting prompt coincidence events with the detectors at (157.6°) versus those at (75.5° and 104.5°). The DCO ratio is defined as $R_{DCO} = I_\gamma(157.6°, \approx 90°)/I_\gamma(\approx 90°, 157.6°)$, where $I_\gamma(157.6°, \approx 90°)$ is the intensity of a transition measured by the detectors at 157.6° by gating on the detectors at ≈ 90°, and $I_\gamma(\approx 90°, 157.6°)$ is the intensity of a transition measured by the detectors at ≈ 90° by gating on the detectors at 157.6°. The obtained DCO ratio depends on the multipolarity of the gating transition. The typical R_{DCO} values obtained by gating on a stretched quadrupole transition are ≈1 for stretched quadrupole and ≈0.46 for dipole transitions, while those obtained by gating on a stretched dipole transition are ≈ 1 for a dipole and ≈ 2.1 for a quadrupole transition.

In order to firmly establish the parity of the newly identified bands, linear polarization measurements were performed for a few clean, strong, linking γ-ray transitions as described in Refs. [29]. Two matrices were constructed with events in which γ-rays were scattered between the crystals of a clover detector in parallel (perpendicular) directions relative to the beam direction on one axis, and γ-rays detected by all detectors on the other axis. The polarization asymmetry is defined by

$$A_P = \frac{a(E_\gamma)N_\perp - N_\parallel}{a(E_\gamma)N_\perp + N_\parallel}, \quad (1)$$

where $N_\perp$ and $N_\parallel$ are the number of coincidence counts for a γ-ray of interest obtained by setting the same gates in the two asymmetric matrices on the all-detector axis. The $a(E_\gamma)$ denotes the normalization factor due to the asymmetry in the response of the perpendicular and parallel clover segments.

B. Results

The experimental information on the γ-ray transitions of ^{119}Cs, including the results that we published previously in Refs. [14, 15] and the new ones reported here, is given in the Appendix.

The complete level scheme of ^{119}Cs is shown in three separate figures, one with the negative-parity states (Fig. 1), and two with the positive-parity states (Figs. 2 and 3). A zoom on the low-spin part of the level scheme is also given in Fig. 4. The band labels are in agreement with those employed in Refs. [14, 15] in which partial level schemes have been published: Bands 1, 3, 4 and 5 in Ref. [15] which reported the evidence of oblate-prolate coexistence close to the ground state, and Bands 8, 9 and 10 in Ref. [14] which reported chiral doublet bands. Double-gated spectra showing the transitions of the six newly identified Bands γ, 2, 4', 5', 6 and 7 reported in the present work are given in Figs. 5, 6 and 7. In panel (a) of Fig. 5 one can see a clean spectrum of Band γ constructed by doubly-gating on selected transitions, showing strong transitions between the even-spin states and weaker ones between the odd-spin non-yrast states above the $37/2^-$ state. In panels (b) and (c) of Fig. 5 are shown spectra of the two signature partners of Band 2, with the transitions of the $\alpha = -1/2$ cascade much stronger than those of the $\alpha = +1/2$ cascade. The highest transitions of 1857 and 1406 keV observed in the two cascades of Band 2 are clearly seen in the two spectra. In Fig. 6 are shown spectra of Bands 4' and 5', which are observed in different spins ranges: Band 4' is built on the $61/2^+$ state, decays only to Band 4 via the 1181-keV transition and is observed up to the $85/2^+$ state depopulated by the 1768-keV transition which is clearly seen in panel (a); Band 5' is much weaker, decays only to Band 5 and is observed up to the the $45/2^+$ state depopulated by the 982-keV transition clearly seen in panel (b). Fig. 7 shows clean double-gated spectra of Bands 6 and 7: in panel (a) one can clearly see the in-band transitions, as well as the populating 603-keV and 292-keV transitions from Band 7, and the depopulating 738-, 1508- and 1550-keV transitions; in panel (b) one can see a very clean spectrum of Band 7 up to the highest observed 1805-keV transition.

As all bands reported in the present work are interconnected by γ-ray transitions, we could establish the relative energy of not only the bands with short-lived band-heads, but also of the two long-lived β^+-decaying $3/2^+$ and $9/2^+$ isomers. The 85.7 keV energy of the $9/2^+$ isomer is established by the connecting transitions between Bands 8 and 6, which in turn decays to Band 4 through the 738.1-keV transition. The 110.2 keV energy of the $11/2^-$ band-head of Band 1 is established by several connecting transitions to Bands 4 and 6. As Band 1 is depopulated by the observed delayed 87.1-keV transition, an unobserved 23.1-keV transition in cascade with the 87.1-keV transition should exist, which defines a state with tentative spin-parity $I^\pi = (7/2^+)$ and energy that can be either 23.1 keV or 87.1 keV. One can exclude the 23.1-keV energy of this $(7/2^+)$ state based on the long half-life of the $9/2^+$ 85.7-keV isomer which would then have the possibility to decay internally through γ emission and therefore a much shorter half-life. We therefore propose a $(7/2^+)$ state at 87.1(2) keV, which is higher by ≈ 1 keV than the 85.7-keV energy of the β-decaying $9/2^+$ band-head of Band 8. One should note that the energy of the $9/2^+$ band-head is established with a error of ≈ 2 keV, which results from the cumulative errors of the energies of about 20 transitions on the path from the ground state up to the $33/2^+$ band-head of Band 7 and down to the $9/2^+$ band-head of Band 8. However, we are confident on the estimated energy of 86 keV for the $9/2^+$ band-head of Band 8, because it becomes the lowest excited state which cannot decay internally through γ emission to the $3/2^+$ ground state.

One of the most important results of the present work is the determination of the ground state of ^{119}Cs, which we assign as the long-lived $T_{1/2} = 30.4(1)$ s, β^+-decaying

$3/2^+$ state [12]. This is the state with the lowest energy in the level scheme, which we assign as the ground state (see Fig. 4). The previously assigned $9/2^+$ ground state [12] becomes an excited state with an energy of 85.7 keV. The spins and parities of the low-lying $3/2^+$ and $1/2^+$ states at 103 and 112 keV, respectively, are assigned based on the intensity balance of the states, as well as on the systematics of the low-lying states in heavier odd-even Cs nuclei [11]. The $1/2^+$ state at 112-keV can in fact correspond to the $1/2^+$ ground states of the heavier odd-even ^{123,125,127}Cs nuclei, which becomes excited in the lighter ^{119,121}Cs nuclei with $3/2^+$ ground states.

Band 1, previously known up to spin $35/2^-$ [7], was extended up to spin $(67/2^-)$ in Ref. [15]. A half-life of $T_{1/2} = 55(5)$ μs was also deduced in Ref. [15] for the 110-keV $11/2^-$ band-head from the fit of the delayed 87-keV transition detected at the MARA focal plane in coincidence with transitions of Band 1 measured at the target position with JUROGAM 3. The $11/2^-$ band-head decays through the cascade of delayed (23) keV (unobserved) and 87 keV transitions to the $3/2^+$ ground state, and via the delayed (25)-keV transition (unobserved) to the $9/2^+$ long-lived isomer. A time window of 500 μs, much longer than the measured half-life of the isomer, was used in the coincidence analysis. The isomeric character of the $11/2^-$ state can be induced by the low-energy (23)- and (25)-keV unobserved transitions. In fact, the assigned $(7/2^+)$ spin and parity to the 87-keV state, leads to an $M2$ character for the (23)-keV transition and an $E1$ character of the (25)-keV transition. The Weisskopf estimates of these highly converted $M2$ and $E1$ transitions lead to a lifetime of the order of several tens of microseconds, which is in agreement with the measured half-life. The Weisskopf estimate for the 87-keV $E2$ transition is about 1 μs, which is much shorter than the measure half-life of 55 μs. The band decaying to the $15/2^-$ state of Band 1 was very weakly populated. Therefore the spins and parities of the states could not be established. Based on the calculations described in Ref. [15], we assigned it as the unfavored signature partner of Band 1.

Band γ is newly observed. It feeds states up to spin $23/2^-$ of Band 1, the $19/2^-$ state of Band 2, and is observed up to spin 55/2. A cascade of three transitions of 1005, 1100 and 1191 keV form a band which decays via the $M1/E2$ 964-keV transition to the $35/2^-$ state of Band γ.

Band 2 is composed of two long cascades of $E2$ transitions built on the $15/2^-$ and $17/2^-$ states, at excitation energy of 1258 and 1264 keV, respectively. The two cascades evolve to very high spins of 83/2 and 65/2, and exhibit a large signature splitting, indicating the occupation a low-Ω $h_{11/2}$ orbital. The cascade built on the $15/2^-$ state decays via many $M1/E2$ and $E2$ transitions to levels of Band 1, Band γ and the intermediate $(15/2^-)$ state which in turn decays to Band 1 via the 499-keV transition. The cascade built on the $17/2^-$ state decays to the yrast cascade of Band 2 built on the $15/2^-$ state, as well as to Band 1 and Band γ. The negative parity of the band is firmly established by five $E2$ out-of-band transitions towards Band 1. A $67/2^-$ state with an energy smaller by 18 keV from the state with the same spin of Band 2, which is fed from the $71/2^-$ state and decays to the $63/2^-$ state of Band 2, has been also identified.

Band 3 has been discussed in Ref. [15]. It is based on the 670-keV $11/2^-$ state which decays through a cascade of transitions towards the $3/2^+$ ground state. No transitions towards other low-lying states were observed. The intensity of the 268-, 237-, and 139-keV transitions depopulating the $11/2^-$ band-head is a factor of 16 lower than the intensity of the populating transitions, indicating an isomeric character of the $11/2^-$ band-head, with a lifetime in the range of tens of nanoseconds. The assigned negative parity of Band 3 is not firmly established, because the 294-keV transition is very weak and the (26)-keV transition to the 643-keV $9/2^+$ state is not observed. It is instead supported by the strongly-coupled character of the band which implies the occupation of the high-Ω $\pi h_{11/2}[505]11/2^-$ orbital close to the Fermi surface for oblate deformation [15]. The decay of Band 3 only towards the three $5/2^+$, $7/2^+$ and $9/2^+$ states below the band-head, and the lack of connecting transitions between these states and the other positive-parity states, strongly suggests that these states are also based on oblate shapes.

Bands 4 has been discussed in Ref. [15]. The statistics did not allow to extract the character of the connecting transitions to Band 1. The assigned positive parity is based on the properties of the band, which, being composed of only one cascade of $E2$ transitions, indicates the occupation of the $\alpha = 1/2$ signature partner of the low-Ω $\pi[420]1/2^+$ orbital.

Band 4' composed of six $E2$ transitions has been observed in coincidence with Band 4. It decays through the 1181-keV transition to the $57/2^+$ state of Band 4. The assigned spins and positive parity to the band are based on the R_{ac} ratios of the observed transitions which are compatible with $E2$ character.

Band 5' composed of seven $E2$ transitions has been observed in coincidence with the transitions of Band 5 below spin $17/2^+$. The assigned spins and positive parity to the band are based on the R_{ac} ratios of the observed transitions which are compatible with $E2$ character.

Band 6 is composed of dipole and one crossover quadrupole transitions, and is observed between spin $21/2^+$ and $33/2^+$. It decays to the $19/2^-$ state of Band 1, to the $17/2^+$ and $21/2^+$ states of Band 4, to the $27/2^+$ and $29/2^+$ states of Band 8, and is fed by the 292- and 603-keV $M1/E2$ transitions from the positive-parity Band 7. The positive parity of Band 6 is firmly established by the 738-keV and 887-keV $E2$ transitions towards the $21/2^+$ and $17/2^+$ states of Band 4, respectively.

Band 7 is a long cascade of twelve $E2$ transitions, which decays to Bands 6 and 8. The $E2$ character of the 704-keV transition towards the $29/2^+$ state of Band 8 fixes the positive-parity of the band.

Bands 8, 9 and 10 have been discussed in Ref. [14] . The lowest lying state of Band 8 is at an excitation energy of 85.7 keV, determined by the connecting transitions to Bands 6 and 7, which in turn are firmly connected with the $3/2^+$ ground state. Bands 9 and 10 decay to Band 8 through several transitions, among which there are two $E2$ transitions from Band 9 and four $E2$ transitions from Band 10 which fix their positive parity.

III. DISCUSSION

Selected experimental results on ^{119}Cs have been already discussed in our recently published articles, Refs. [14, 15]. In the present work we briefly describe the interpretation of the previously published bands, and discuss in more detail the new reported bands.

Bands 1, 3, 4 and 5 have been discussed in Ref. [15], while Bands 8, 9 and 10 have been discussed in Ref. [14]. Bands 8 and 9 are nearly degenerate and have similar moments of inertia (MOI), while Band 10 has a MOI very similar to that of Band 1. Calculations using 3D TAC-CDFT and PNC-CSM have been employed to determine the deformation and to investigate the band configurations, respectively. Bands 8 and 9 have been interpreted as chiral partner bands built on a three-quasiparticle configuration involving three protons, two in the $\pi h_{11/2}$ subshell and one in the strongly-coupled $\pi g_{9/2}[404]9/2^+$ orbital. The calculations showed that the angular momenta of the two $h_{11/2}$ protons reorient from the short to the intermediate axis, in a plane orthogonal to the angular momentum of the strongly-coupled $g_{9/2}$ proton which keeps aligned along the long axis. The total spin of the three protons and of the core points in 3D, inducing the breaking of the chiral symmetry and giving rise to nearly degenerate doublet bands. This was the first observation of chiral bands built on a configuration with only protons in the transient backbending regime. We called this new type of chiral bands *Revolving Chiral Doublet* ($R\chi D$) bands. Band 10, which has a MOI similar to that of Band 1 built on the $\pi[541]3/2^-$ orbital, was observed only above the alignment of a pair of neutrons and was assigned to the $\pi[541]3/2(\alpha=+1/2)\otimes\nu^2[413]5/2[523]5/2$ configuration.

In the present work we investigate the possible configurations of the other observed bands using PNC-CSM calculations similar to those reported in Refs. [14, 15]. The phenomenological Nilsson potential is adopted for the mean field [16], with parameters κ and μ taken from Ref. [30], and effective monopole pairing strengths of 0.8 MeV for protons and 0.6 MeV for neutrons. This model was recently used to successfully describe the band structure in rare-earth nuclei [17]. We do not discuss the γ band which cannot be described by the PNC-CSM calculations. Single-particle Routhian diagrams as a function of rotational frequency for prolate and oblate deformations which were used to guide the search of the closest quasiparticle orbitals to the proton and neutron Fermi surfaces are shown in Fig. 9. Since no blocking technique is used in the PNC method, the occupation probabilities of each orbital, which are obtained from the many-body wave-function, change with rotational frequency. The wave functions are mixed in the high-spin region, which can be seen from the occupation probabilities of each orbital close to the Fermi surface. As an example, in Fig. 8 shows the neutron occupation probabilities of the orbitals involved in the $\pi^3[420]1/2[550]1/2[541]3/2\otimes\nu^2[411]3/2[413]5/2$ configuration of Band 7 (see Fig. 15) which obviously change. The situation is more complicated for the proton occupation probabilities of Band 7.

An important issue in the interpretation of the observed bands is the adopted deformation. The calculations have been performed assuming axial symmetric shapes, which for nuclei with limited triaxiality of $\gamma\approx 10^\circ$ like ^{119}Cs [14], is a good approximation. The spectroscopic quadrupole moment has been measured for the band-head of Band 8 built on the $\pi[404]9/2^+$ orbital and lead to $\varepsilon_2=0.32$ ($\beta=0.34$) [13]. However, the calculated ground-state deformation, like for example using the finite-range droplet model (FRDM) [31], is significantly smaller ($\varepsilon_2=0.25, \varepsilon_4=-0.02, \gamma=15^\circ$), corresponding to an axial deformation of $\varepsilon_2=0.23$. We performed calculations for the two deformations and found that the results for the smaller deformation $\varepsilon_2=0.23$ are in clear disagreement with the experimental data (see Fig. 10). We therefore adopted the $\varepsilon_2=0.32$ deformation for all prolate bands, excepting the negative-signature partner of Band 2 for which a slightly smaller deformation of $\varepsilon_2=0.30$ leads to a better agreement with the observed crossing at $\hbar\omega\approx 0.3$ MeV (see Fig. 11). For the oblate Band 3 we adopted a deformation of $\varepsilon_2=-0.17$ resulting from 2D TAC-CDFT calculations [15]. The assigned configurations and adopted deformations of all bands are listed in Table I.

The choice of the larger deformation is reasonable in nuclei like ^{119}Cs which has the Fermi surface close to high-j low-Ω orbitals like $\pi h_{11/2}[550]1/2^-$ and $\pi h_{11/2}[541]3/2^-$, which have very strong deformation driving effects and can induce larger deformations. In fact, in the case of Band 1, a backbending due to the alignment of a pair of $h_{11/2}$ neutrons is calculated at $\hbar\omega\approx 0.3$ MeV if one uses a deformation of $\varepsilon_2=0.23$, which is not observed experimentally (see Fig. 10). A good agreement with experiment is only obtained if one uses a larger deformation of $\varepsilon_2=0.32$, for which the proton alignment becomes very smooth (similar to the effect observed for the $\pi[541]1/2^-$ orbital in rare-earth nuclei [17]). As one can see in Fig. 9a, for deformation $\varepsilon_2=0.32$ and rotational frequency $\hbar\omega\approx 0.3$ MeV, the $\pi[541]3/2^-$ orbital is closer to the $Z=55$ Fermi surface than the $\pi[550]1/2^-$ orbital. Therefore, based on the PNC-CSM calculations, the $\pi[541]3/2^-$ orbital should be assigned to the yrast negative-parity Band 1, even if it is strongly mixed with the $\pi[550]1/2^-$ one.

For oblate deformation there is only one negative-

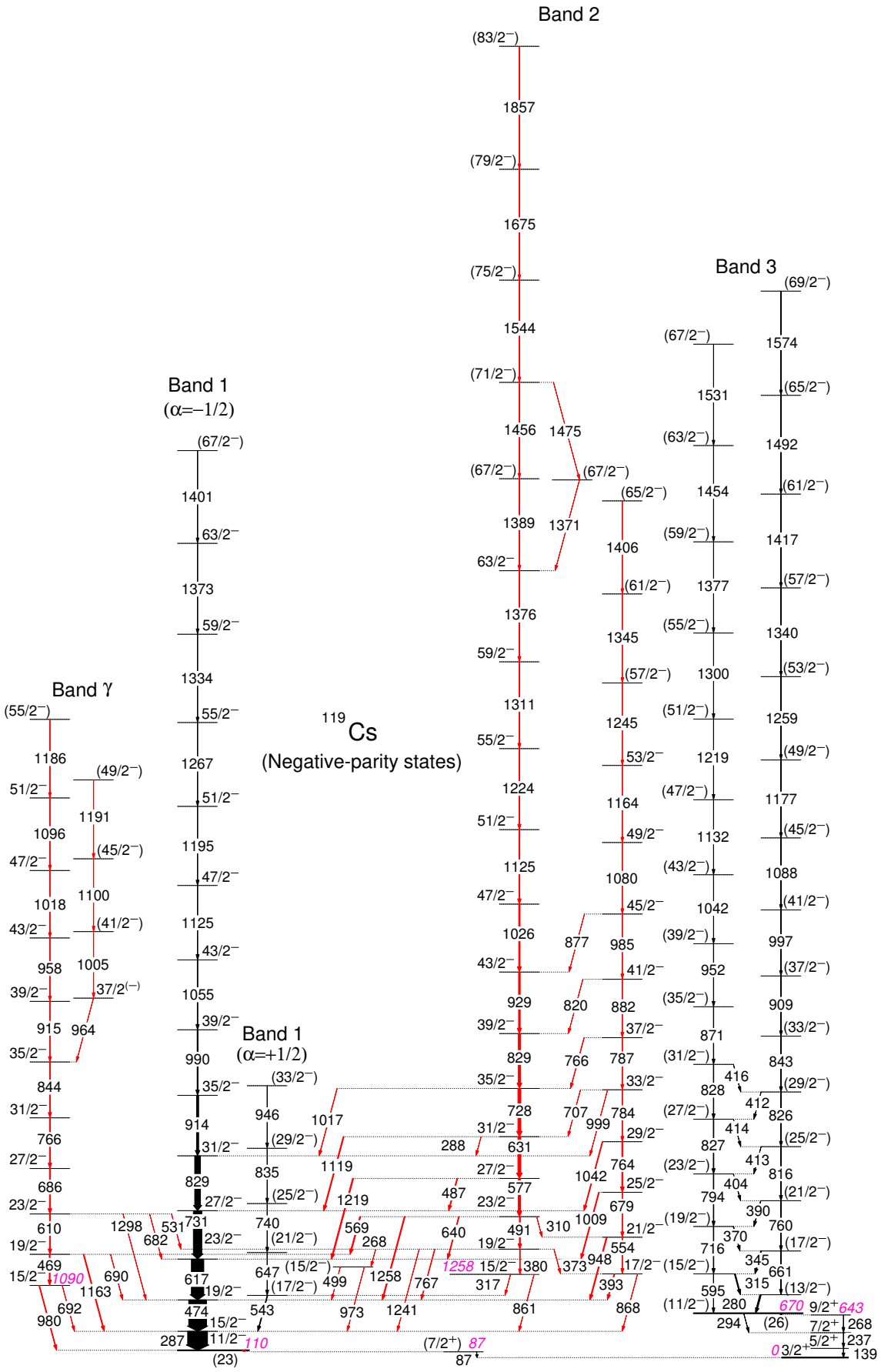

FIG. 1. (Color online) Partial level scheme of ^{119}Cs showing the negative-parity bands. The new transitions are indicated in red, while the transitions reported in Ref. [15] are indicated in black. The isomeric levels are indicated with thick lines. Energies of levels with some relevance are shown in purple italics figures.

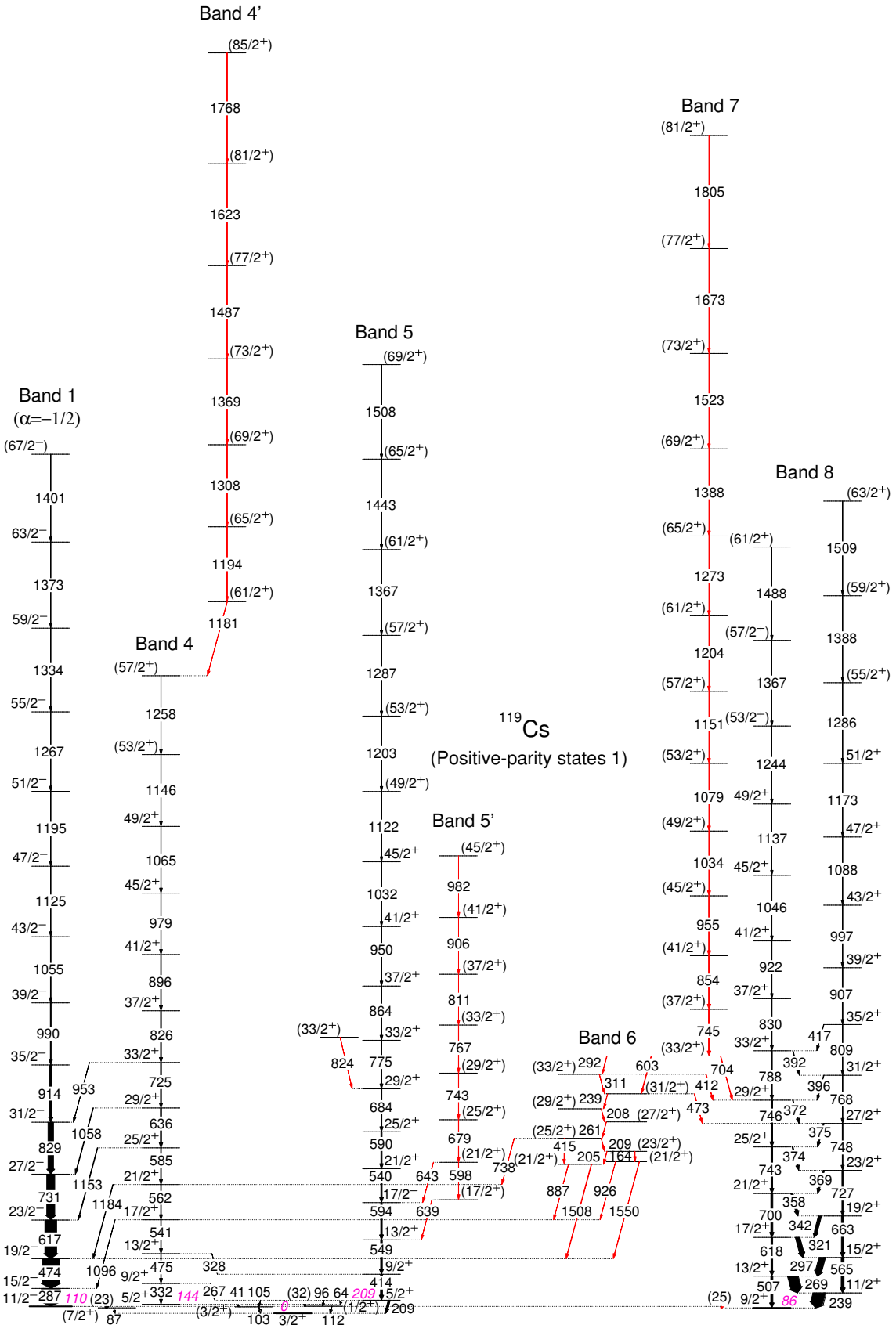

FIG. 2. (Color online) Partial level scheme of ^{119}Cs showing the first part of the positive-parity states, and the negative-parity Band 1 to which Band 4 decays via several transitions. The new transitions are indicated in red, while the transitions reported in Ref. [15] are indicated in black. The isomeric levels are indicated with thick lines. Energies of levels with some relevance are shown in purple italics figures.

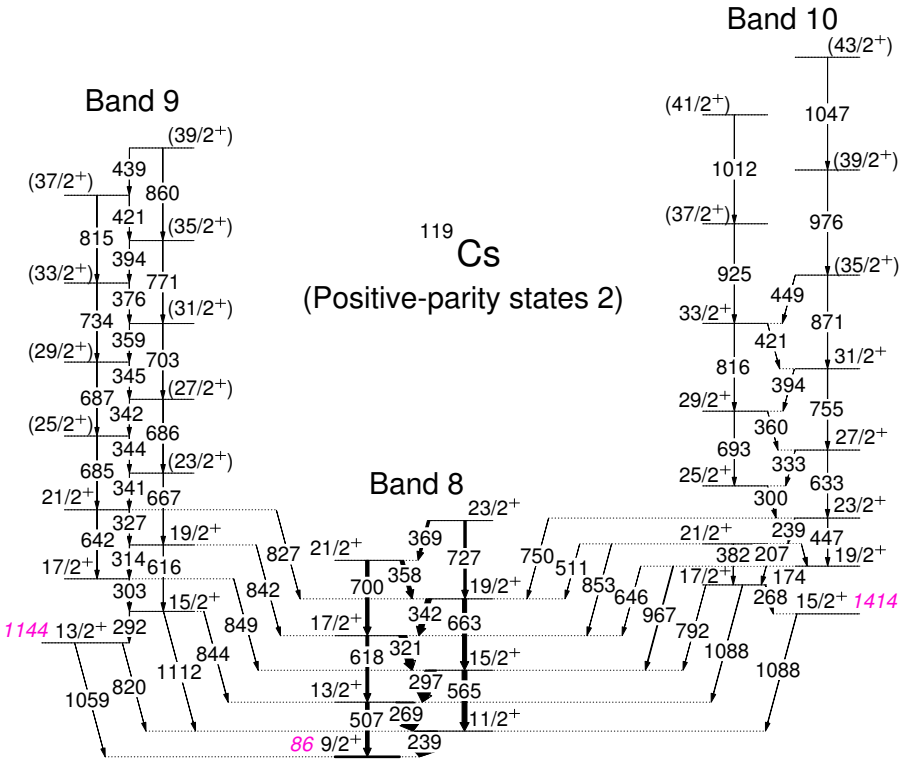

FIG. 3. (Color online) Partial level scheme of ^{119}Cs showing the positive-parity states of Bands 8, 9 and 10 previously published in Ref. [14]. Energies of levels with some relevance are shown in purple italics figures.

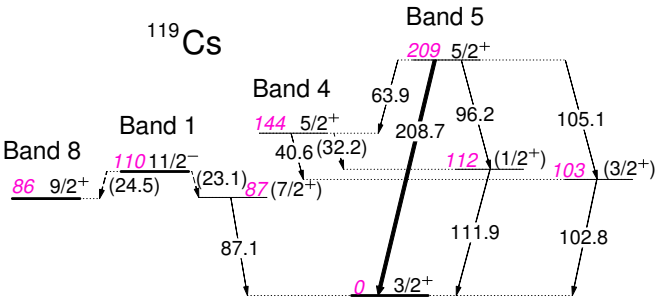

FIG. 4. (Color online) Zoom on the low-spin part of the level scheme.

parity orbital, $\pi[505]11/2^-$, and three positive-parity orbitals, $\pi[404]7/2^+$, $\pi[413]5/2^+$, and $\pi[402]5/2^+$, which are close to the $Z = 55$ Fermi surface (see Fig. 9c). The negative-parity orbital was assigned to Band 3, while the positive-parity ones can account for the observed low-lying states to which the oblate Band 3 decays [15].

In the present work we assign configurations to the Bands 2, 4', 5', 6, and 7 which were not discussed previously. Band γ cannot be described by the present PNC-CSM calculations which assumes a rigid axial deformation. It is assigned as γ band based on the comparison with other bands with similar behavior observed in neighboring nuclei. As one can see in Fig. 11, the configuration assigned to Band 2 is similar to that of Band 1, $\pi[541]3/2^-$, which is crossed at $\hbar\omega \approx 0.3$ MeV for the negative-signature partner and at $\hbar\omega \approx 0.4$ MeV for the positive-signature partner by a three-quasiparticle configuration involving two additional neutrons placed in positive-parity orbitals, leading to a $\pi[541]3/2 - \otimes\nu[411]3/2^+[413]5/2^+$ configuration at high spin. For the $\alpha = 1/2$ signature partner, the calculated second alignment at $\hbar\omega \approx 0.7$ MeV induced by neutrons has not been observed experimentally (see Fig. 11b).

Band 4' which feeds the top of Band 4, exhibits a higher MOI and J_x than Band 4, indicating the presence of additional nucleons in its configuration. The best agreement is obtained for the $\pi[420]1/2^+(\alpha = 1/2) \otimes \pi^2([550]1/2^-[541]3/2^-) \otimes \nu^2([541]1/2^-[532]5/2^-)$ configuration (see Fig. 12).

Band 5' decays to the $13/2^+$ and $17/2^+$ states of Band 5. It should have a three-quasiparticle configuration, most probably with one proton placed on the

same positive-parity orbital $\pi[422]3/2^+$ as in the case of Band 5. The first alignment is observed at a frequency of $\hbar\omega \approx 0.30$ MeV which is higher than $\hbar\omega \approx 0.26$ MeV observed in Bands 4 and 5. It should therefore be induced by neutrons which, for a deformation of $\varepsilon_2 \approx 0.32$, align later than $h_{11/2}$ protons. We therefore assign the $\pi[422]3/2^+ \otimes \nu h^2_{11/2}([532]5/2^-[523]7/2^-)$ configuration to Band 5', which is in excellent agreement with the experimental results.

Band 6, composed of dipole and cross-over $E2$ transitions, is populated by transitions from Band 7 and mainly decays to Band 1. One would expect to have involved the $\pi[541]3/2^-$ orbital on which Band 1 is built, and also orbitals present in the five-quasiparticle configuration of Band 7 (see discussion below), in particular the positive-parity neutron orbital $\nu[413]5/2^+$. A configuration involving such low- and high-Ω orbitals can lead to rotation around a tilted axis and give rise to a dipole band like Band 6. However, one cannot expect a very good agreement of the PNC-SCM calculations performed in the present work and the experimental data, because of the adopted axial symmetric shapes and principal axis rotation in PNC-CSM. We performed anyhow calculations for the $\pi[541]3/2^- \otimes \nu^2[413]5/2^+[532]5/2^-$ configuration and compared it with the experimental Band 6 in Fig. 14. One can see that there is a qualitative agreement for the configuration involving the $\pi[541]3/2^-$ ($\alpha = -1/2$) orbital. One can therefore speculate that Band 6 is based on a configuration with one proton in the $\pi[541]3/2^-$ ($\alpha = -1/2$) orbital, and two neutrons in orbitals with positive- and negative-parity. Tilted axis cranking calculations are more adequate for the description of dipole bands and can validate this configuration assignment.

Band 7 is a very long sequence of electric quadrupole transitions, which develops in the spin range from 33/2 to 81/2, and decays to positive-parity states of Bands 6 and 8. We assigned it the five-quasiparticle configuration $\pi^3[550]1/2^-[541]3/2^-[420]1/2^+ \otimes \nu^2[413]5/2^+[413]5/2^+$, which is in good agreement with the experimental data (see Fig. 15). The decay to Band 6 is explained by the presence of $\pi h_{11/2}$ orbitals in the two bands, whereas the decay to Band 8 can be understood by the accidental mixing between the $33/2^+$ states of the two bands.

IV. SUMMARY

Summarizing, the present work reports new results in ^{119}Cs, in particular Band γ, Band 2, Band 4' and Band 5', which together with those reported recently, all resulting from the same high statistics experiment, contribute to the realization of one of the most complete level schemes from low to high spin in proton-rich lanthanide nuclei. The band configurations are discussed within the PNC-CMS formalism, which nicely describe the band patterns, as well as the the contribution of protons and neutrons to the observed alignments. The present results constitute an unique set of spectroscopic information which can be used to test state-of-the-art theoretical models aiming to describe strongly-deformed proton-rich lanthanide nuclei.

V. ACKNOWLEDGMENTS

This work has been supported by the China Scholarship Council (CSC), CSC No. 201804910386. This work has been supported by the Academy of Finland under the Finnish Centre of Excellence Programme (2012-2017), by the EU 7th Framework Programme Project No. 262010 (ENSAR), by the United Kingdom Science and Technology Facilities Council, by the National Research, Development and Innovation Fund of Hungary (Project No. K128947), as well as by the European Regional Development Fund (Contract No. GINOP-2.3.3-15-2016-00034); by the Polish National Science Centre (NCN) Grant No. 2013/10/M/ST2/00427; by the Swedish Research Council under Grant No. 2019-04880; and by the National Natural Science Foundation of China (Grants No. 11505242, No. 11305220, No. U1732139, No. 11775274, and No. 11575255). The use of germanium detectors from the GAMMAPOOL is acknowledged. I.K. was supported by National Research, Development and Innovation Office-NKFIH, contract number PD 124717.

[1] B. Xiong and Y. Wang, Atomic Data and Nuclear Data Tables **125**, 193 (2019).
[2] P. T. Wady *et al.*, Phys. Rev. C **85**, 034329 (2012).
[3] J. F. Smith *et al.*, Phys. Rev. C **73**, 061303 (2006).
[4] J. F. Smith *et al.*, Phys. Rev. C **74**, 034310 (2006).
[5] J. F. Smith *et al.*, Phys. Rev. C **63**, 024319 (2006).
[6] J. F. Smith *et al.*, Phys. Lett. B **406**, 7 (1997).
[7] F. Lidén *et al.*, Nucl. Phys. A **550**, 365 (1992).
[8] B. Cederwall *et al.*, Nucl. Phys. A **542**, 454 (1992).
[9] C. B. Moon, T. Komatsubara, and K. Furuno, Journal Korean Physical Society **38**, 83 (2001).
[10] R. Kumar *et al.*, Phys. Rev. C **72**, 044319 (2005).
[11] A. Gizon *et al.*, Eur. Phys. J. A **8**, 41 (2012).
[12] ENSDF, NNDC Online Data Service, ENSDF database, http://www.nndc.bnl.gov/ensdf/.
[13] C. Thibault *et al.*, Nucl. Phys. A **367**, 1 (1981).
[14] K. K. Zheng *et al.*, chiral bands in ^{119}Cs, to be published.
[15] K. K. Zheng *et al.*, Phys. Lett. B (2021), 10.1016/j.physletb.2021.136645.
[16] J. Y. Zeng, T. H. Jin, and Z. J. Zhao, Phys. Rev. C **50**, 1388 (1994).
[17] Z. H. Zhang, M. Huang, and A. V. Afanasjev, Phys. Rev. C **101**, 054303 (2020).
[18] J. Pakarinen *et al.*, Eur. Phys. J. A **56**, 149 (2020).

[19] J. J. Uusitalo, J. Sarén, J. Partanen, and J. Hilton, Acta Phys. Pol. B **50**, 319 (2019).
[20] J. Sarén *et al.*, Nucl. Instr. Meth. Phys. Res. A **266**, 4196 (2008).
[21] J. Hilton *et al.*, Phys. Rev. C **100**, 014305 (2019).
[22] G. Duchêne *et al.*, Nucl. Instr. Meth. Phys. Res. A **432**, 90 (1999).
[23] C. W. Beausang *et al.*, Nucl. Instr. Meth. Phys. Res. A **313**, 37 (1992).
[24] P. Rahkila, Nucl. Instrum. Meth. Phys. Res. A **595**, 637 (2008).
[25] D. Radford, Nucl. Instrum. Meth. Phys. Res. A **361**, 297 (1995).
[26] D. Radford, Nucl. Instrum. Meth. Phys. Res. A **361**, 306 (1995).
[27] A. Krämer-Flecken, T. Morek, R. M. Lieder, W. Gast, G. Hebbinghaus, H. M. Jäger, and W. Urban, Nucl. Instrum. Meth. Phys. Res. A **275**, 333 (1989).
[28] C. J. Chiara *et al.*, Phys. Rev. C **75**, 054305 (2007).
[29] K. Starosta *et al.*, Nucl. Instrum. Meth. Phys. Res. A **423**, 16 (1999).
[30] T. Bengtsson and I. Ragnarsson, Nucl. Phys. A **436**, 14 (1985).
[31] P. Möller, R. Bengtsson, B. G. Carlsson, P. Olivius, T. Ichikawa, H. Sagawa, and A. Iwamoto, Atomic Data and Nuclear Data Tables **94**, 758 (2008).

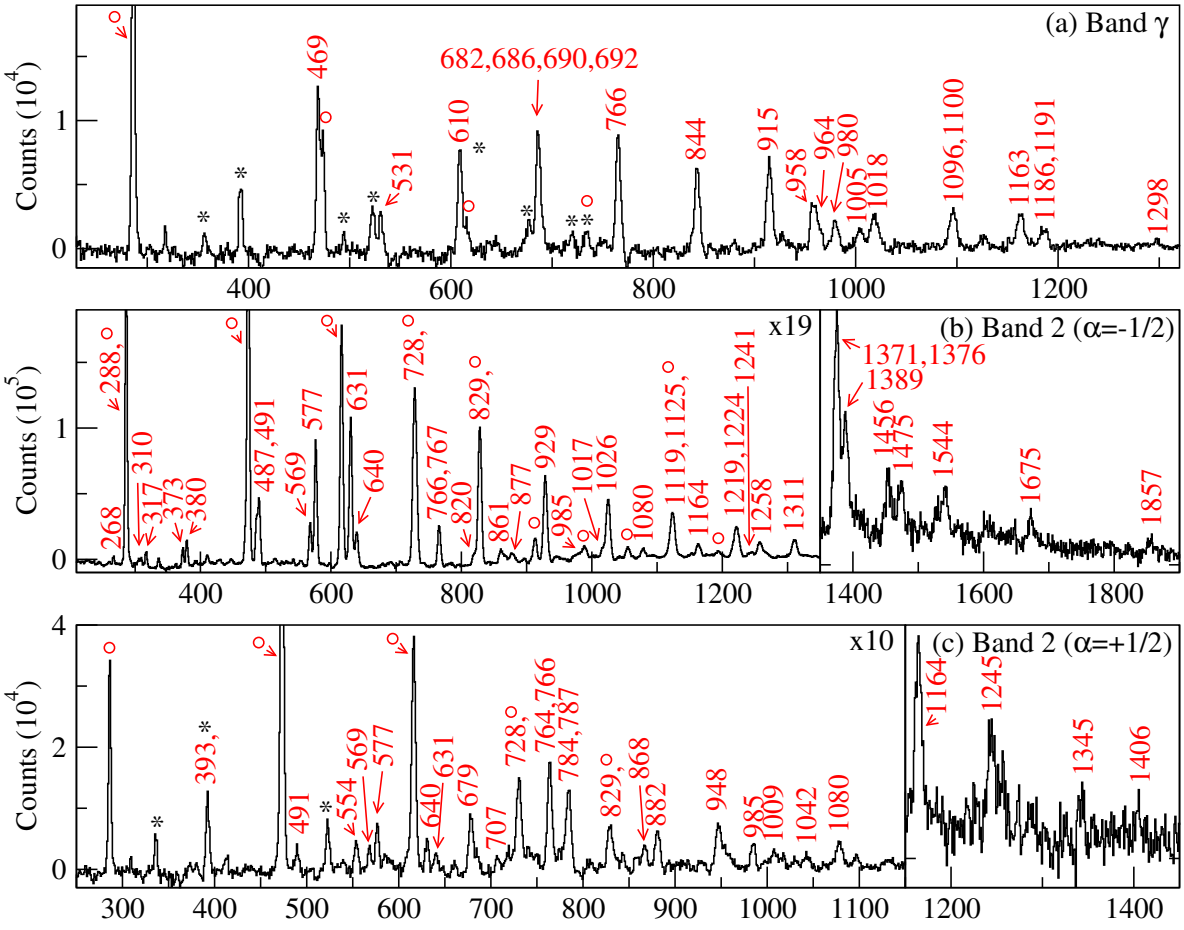

FIG. 5. (Color online) Spectra for Band γ, and the two signature partners of Band 2 of ^{119}Cs obtained from triple coincidences by double-gating on selected transitions using the gate list given below. Peak energies for the newly identified transitions are written in red. Transitions from other nuclei (^{116}Xe, ^{118}Xe, ^{120}Ba) are indicated with an asterisk, while those from other bands in ^{119}Cs are indicated with a red circle. The lists of gating transitions for each spectrum are the following: for Band γ 610, 686, 766, 844, 958, 980, 1018, 1163; for Band 2 (α=-1/2) 287, 380, 491, 577, 631, 728, 829, 1026, 1125, 1224, 1311, 1376, 1456, 1544, 1675 keV; for Band 2 (α=+1/2) 287, 554, 679, 787, 868, 882, 948, 985, 1009, 1042, 1080, 1164, 1245 keV.

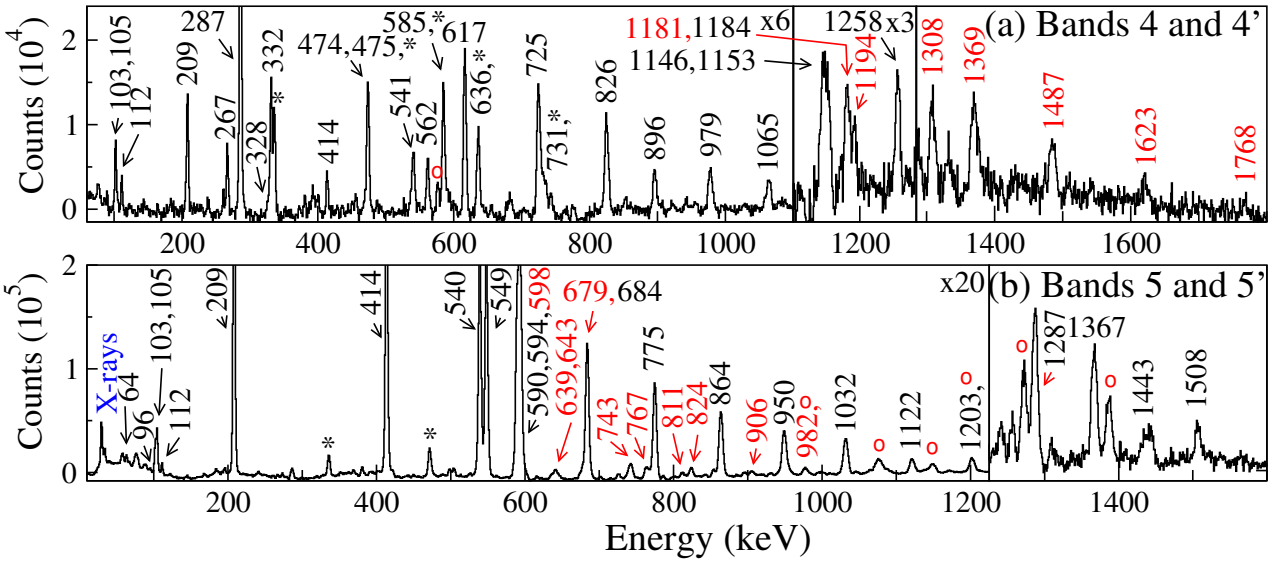

FIG. 6. (Color online) Spectra for Bands 4, 4', 5, 5' of ^{119}Cs obtained from triple coincidences by double-gating on selected transitions. Peak energies for the newly identified transitions are written in red. Transitions from other nuclei (^{116}Xe, ^{119}Ba, ^{120}Ba) are indicated with an asterisk, while those from other bands in ^{119}Cs are indicated with a circle. The lists of gating transitions for each spectrum are the following: for Bands 4 and 4' 475, 541, 562, 636, 896, 979, 1065, 1146, 1153, 1369, 1487 keV; for Bands 5 and 5' 209, 414, 549, 594, 540, 684, 775, 864, 950 keV.

TABLE I. Assigned Nilsson configurations, parity π, and deformations ε_2 to the bands of ^{119}Cs based on PNC-CSM calculations. The configurations include the orbitals occupied at the band-head, as well as those occupied after alignments and crossings at higher spin.

Band	Configuration	1^{st} crossing	($\hbar\omega$)	2^{nd} crossing	($\hbar\omega$)	π	ε_2
1	$\pi[541]3/2^-$	$\nu^2 h_{11/2}$	(0.45)	$\nu^2(g_{7/2}, d_{5/2})$	(0.70)	−	0.32
2	$\pi[541]3/2^-(\alpha = 1/2)$	$\nu^2(g_{7/2}, d_{5/2})$	(0.36)			−	0.30
2	$\pi[541]3/2^-(\alpha = -1/2)$	$\nu^2(g_{7/2}, d_{5/2})$	(0.30)	$\nu^2(g_{7/2}, d_{5/2})$	(0.70)	−	0.32
3	$\pi[505]11/2^-$	$\nu^2 h_{11/2}$	(0.38)			−	-0.17
4	$\pi[420]1/2^+(\alpha = 1/2)$	$\pi^2 h_{11/2}$	(0.26)	$\nu^2 h_{11/2}$	(0.40)	+	0.32
4'	$\pi[420]1/2^+(\alpha = 1/2) \otimes \pi^2(h_{11/2}) \otimes \nu^2(h_{11/2})$					+	0.32
5	$\pi[422]3/2^+(\alpha = 1/2)$	$\pi^2 h_{11/2}$	(0.26)	$\nu^2 h_{11/2}$	(0.50)	+	0.32
5'	$\pi[422]3/2^+(\alpha = 1/2) \otimes \nu^2 h_{11/2}$					+	0.32
6	$\pi[541]3/2^- \otimes \nu^2(h_{11/2} g_{7/2})$					+	0.32
7	$\pi[420]1/2^+(\alpha = 1/2) \otimes \pi^2 h_{11/2} \otimes \nu^2(g_{7/2}, d_{5/2})$					+	0.32
8	$\pi[404]9/2^+$	$\pi^2 h_{11/2}$	(0.36)			+	0.32
9	$\pi[404]9/2^+$	$\pi^2 h_{11/2}$	(0.30)			+	0.32
10	$\pi[541]3/2^- \otimes \nu^2(h_{11/2} g_{7/2})$					+	0.32

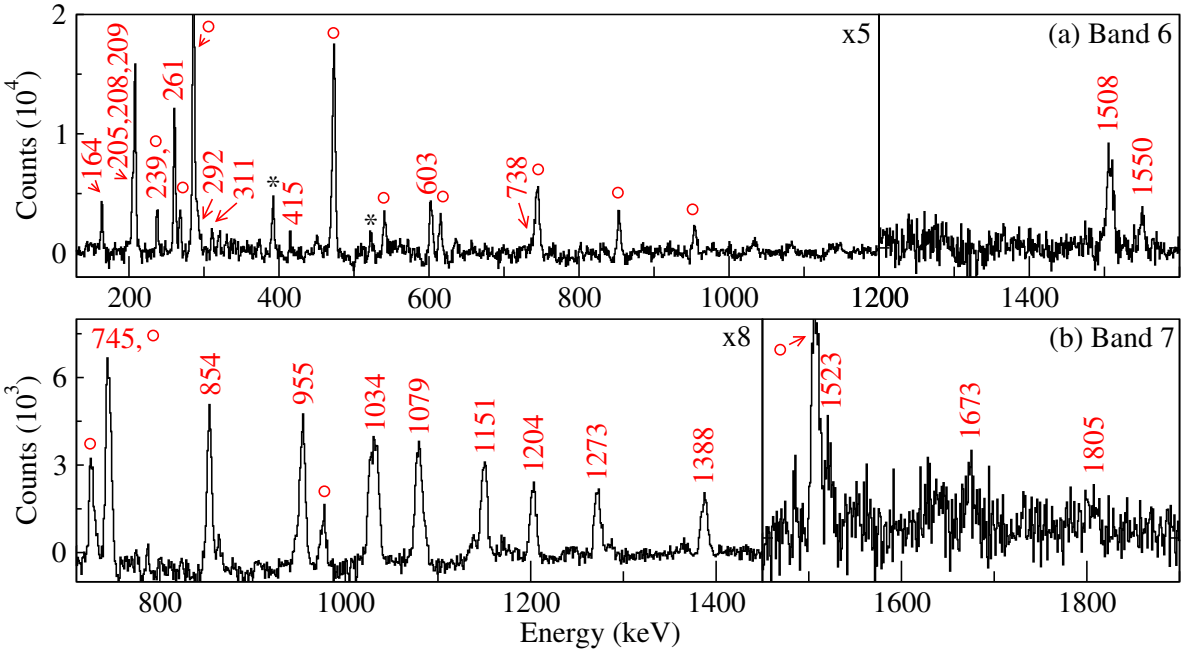

FIG. 7. (Color online) Spectra for Bands 6 and 7 of ^{119}Cs obtained from triple coincidences by double-gating on selected transitions. Peak energies for the newly identified transitions are written in red. Transitions from other nuclei (^{116}Xe, ^{119}Ba, ^{120}Ba) are indicated with an asterisk, while those from other bands in ^{119}Cs are indicated with a circle. The lists of gating transitions for each spectrum are the following: for Band 6 164, 205, 209, 261, 311, 603, 1508, 1550 keV; for Bands 7 745, 854, 955, 1034, 1151, 1204, 1273, 1388, 1523, 1673 keV.

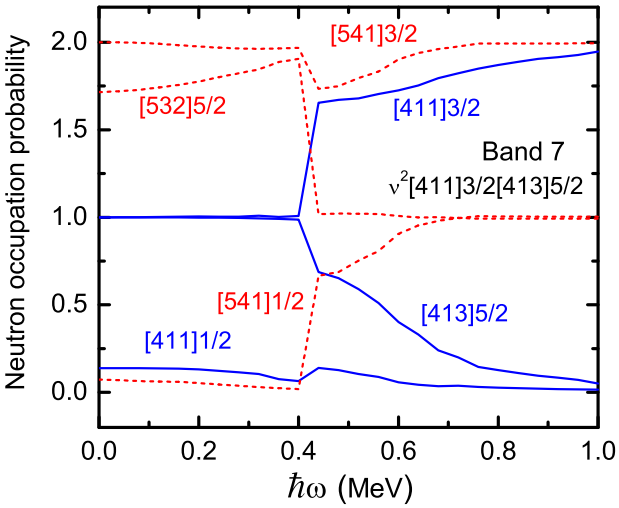

FIG. 8. (Color online) Neutron occupation probabilities of the orbitals involved in the $\pi^3[420]1/2[550]1/2[541]3/2 \otimes \nu^2[411]3/2[413]5/2$ configuration assigned to Band 7. The occupation probability is obtained by adding the occupation probabilities of the two signatures of a given orbital. It is 2 (0) if the orbital is fully occupied (empty), and is 1 if one particle with a given signature is present.

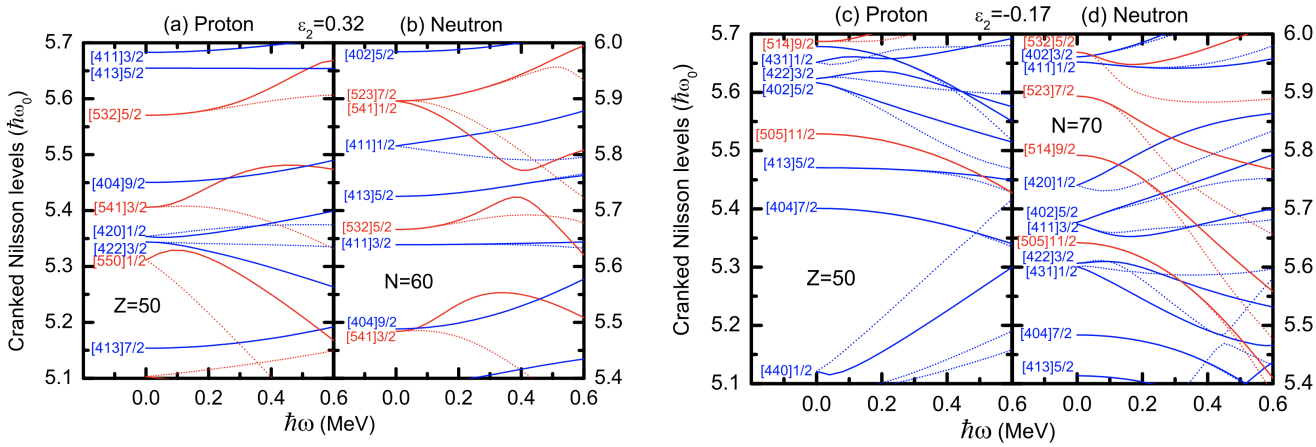

FIG. 9. (Color online) Single-particle Routhians located in the vicinity of the Fermi level of ^{119}Cs as a function of rotational frequency for: a) and b) axial prolate deformation of $\varepsilon_2 = 0.32$; c) and d) axial oblate deformation of $\varepsilon_2 = -0.17$. Positive (negative) parity Routhians are shown by blue (red) lines. Solid (dotted) lines are used for signature $\alpha = +1/2$ ($\alpha = -1/2$).

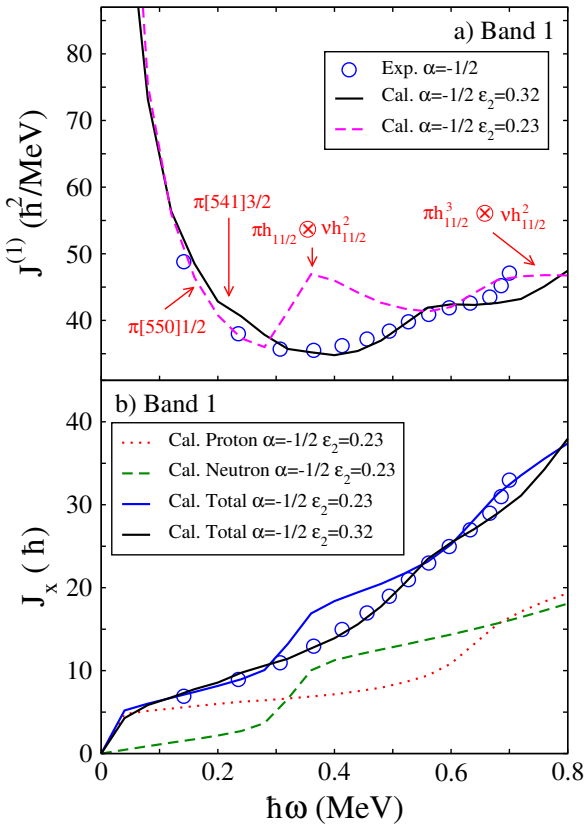

FIG. 10. (Color online) a) Moment of inertia $J^{(1)}$, b) projection of the angular momentum on the cranking axis J_x for the $\alpha = -1/2$ signature partner of Band 1 calculated using the PNC-CSM model for the two deformations $\varepsilon_2 = 0.23$ and $\varepsilon_2 = 0.32$.

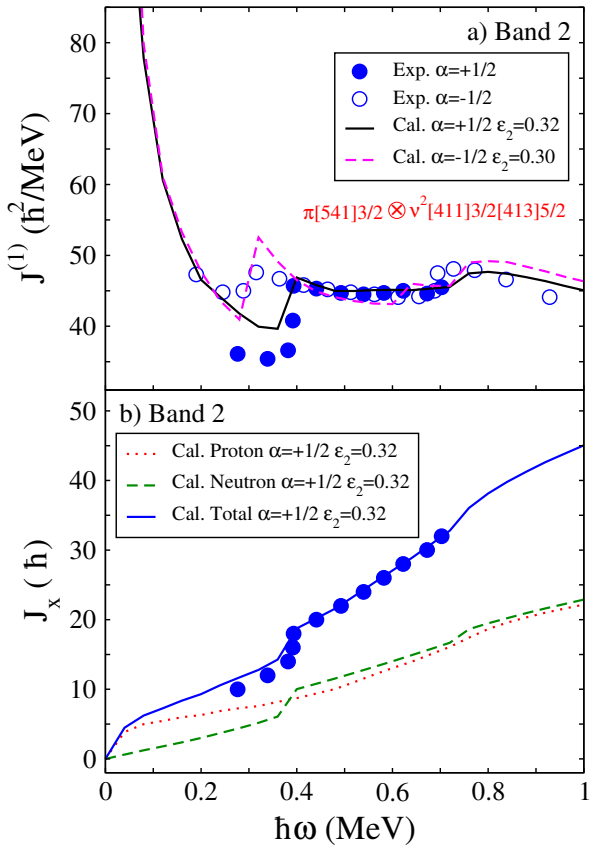

FIG. 11. (Color online) a) Moment of inertia $J^{(1)}$, b) projection of the angular momentum on the cranking axis J_x for Band 2 of ^{119}Cs calculated using the PNC-CSM model. The states with signature $\alpha = +1/2$ and $\alpha = -1/2$ are drawn with filled and open symbols, respectively.

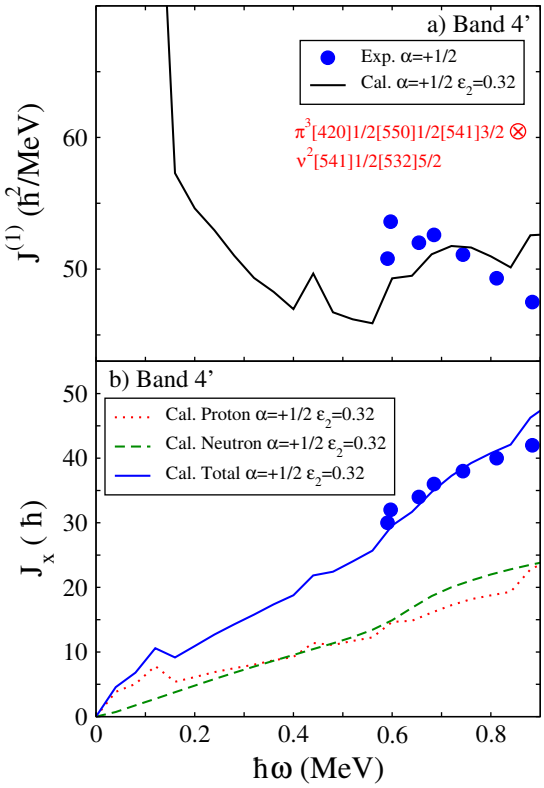

FIG. 12. (Color online) The same as in Fig. 11, but for Band 4'.

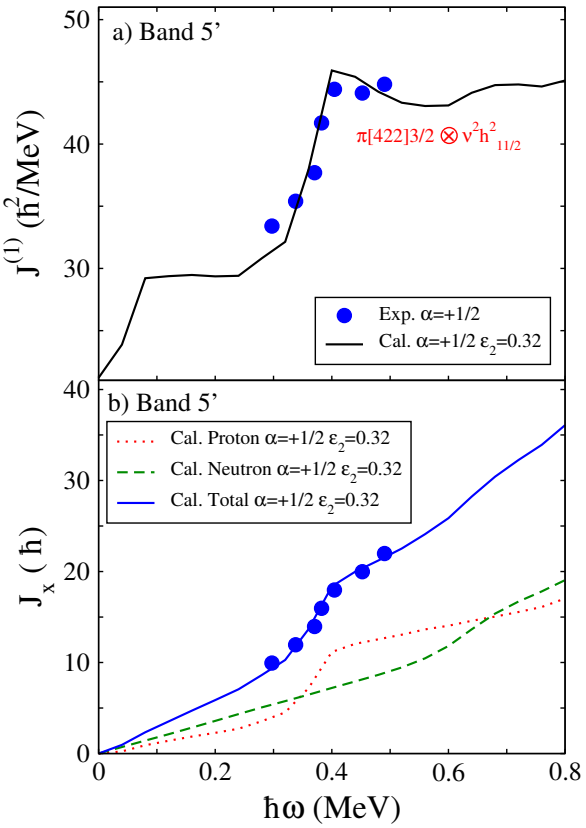

FIG. 13. (Color online) The same as in Fig. 11, but for Band 5'.

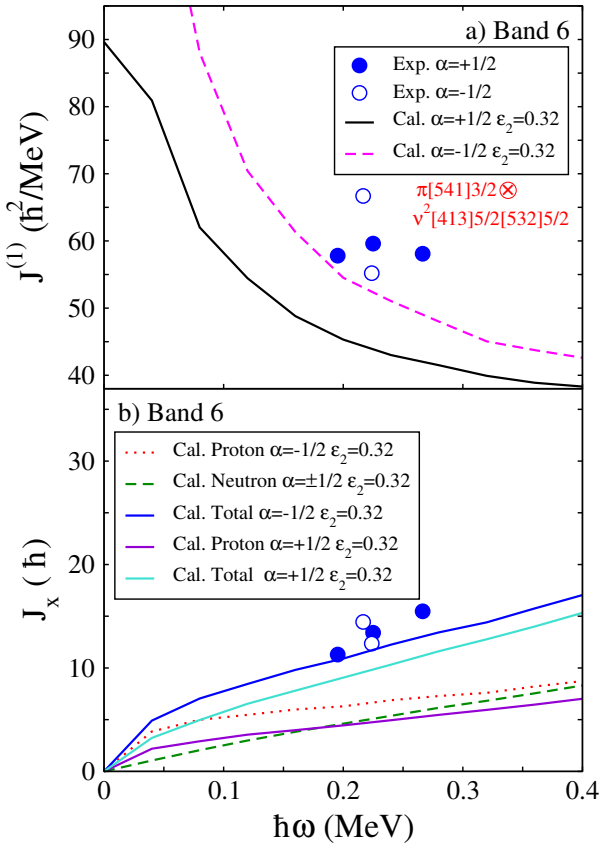

FIG. 14. (Color online) The same as in Fig. 11, but for Band 6.

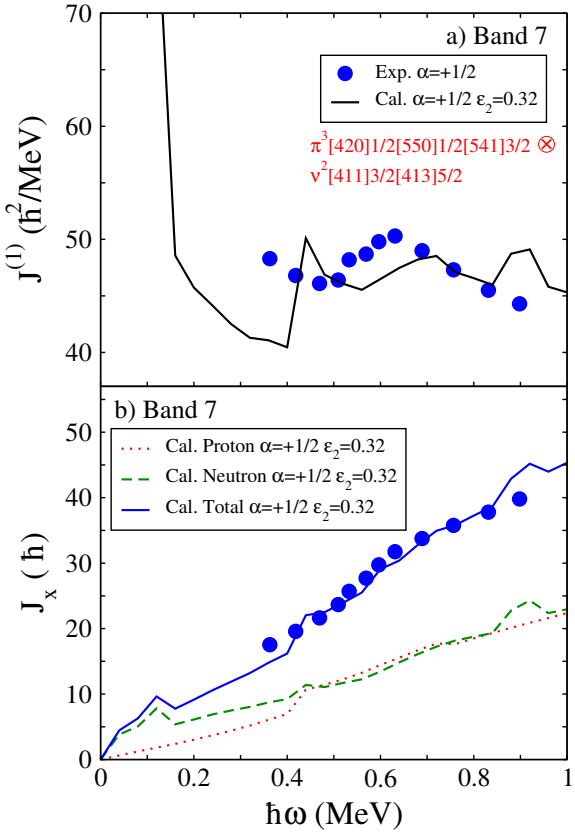

FIG. 15. (Color online) The same as in Fig. 11, but for Band 7.

VI. APPENDIX

Table with experimental information on the γ-ray transitions of ^{119}Cs obtained in the present experiment.

TABLE II. Experimental information including the γ-ray energies E_γ, energies of the initial levels E_i, relative intensities I_γ, anisotropies R_{DCO} and/or R_{ac}, parameter a_2, parameter a_4, polarization asymmetries A_P extracted following the prescription of Ref. [29], mixing ratios δ, multipolarities, and the spin-parity assignments of the initial and final states connected by the given γ ray in ^{119}Cs. The transitions listed with increasing energy are grouped in bands. The deduced values for R_{DCO} with a stretched quadrupole gate are ≈1 for stretched quadrupole and ≈0.46 for dipole transitions, while the ratio is close to 1 for a dipole and 2.1 for a quadrupole transition when the gate is set on a dipole transition. The R_{ac} values for stretched dipole and quadrupole transitions are ≈0.8 and ≈1.4, respectively.

E_γ (keV)[a]	E_i (keV)	I_γ^b	R_{DCO}^c	R_{ac}^d	a_2	a_4	A_P	δ	Mult.	$J_i^\pi \rightarrow J_f^\pi$
Band γ										
469.4	1559.8	46(11)	1.0(3)[e]				0.03(1)		$E2$	$19/2^- \rightarrow 15/2^-$
609.9	2169.5	45(7)	0.9(2)[e]				0.15(8)		$E2$	$23/2^- \rightarrow 19/2^-$
686.3	2855.8	51(12)	0.9(3)[e]				0.2(1)		$E2$	$27/2^- \rightarrow 23/2^-$
765.6	3621.4	46(12)	1.2(3)[e]				0.03(2)		$E2$	$31/2^- \rightarrow 27/2^-$
843.8	4465.2	35(9)	1.1(2)[e]				0.07(6)		$E2$	$35/2^- \rightarrow 31/2^-$
915.2	5380.4	19(6)	1.0(2)[e]						$E2$	$39/2^- \rightarrow 35/2^-$
958.0	6338.4	14(5)	1.1(3)[e]						$E2$	$43/2^- \rightarrow 39/2^-$
964.3	5429.5	7(3)	0.7(5)[e]	0.9(3)					$(M1/E2)$	$37/2^{(-)} \rightarrow 35/2^-$
1004.7	6434.2	5(4)		1.5(5)					$(E2)$	$(41/2^-) \rightarrow 37/2^{(-)}$
1018.4	7356.8	12(5)	0.9(2)[e]						$E2$	$47/2^- \rightarrow 43/2^-$
1096.4	8453.2	9(4)	1.0(4)[e]						$E2$	$51/2^- \rightarrow 47/2^-$
1099.7	7533.9	4(3)							$(E2)$	$(45/2^-) \rightarrow 41/2^{(-)}$
1186.3	9639.5	5(2)		1.3(3)					$(E2)$	$(55/2^-) \rightarrow 51/2^-$
1191.0	8724.9	3(3)							$(E2)$	$(49/2^-) \rightarrow (45/2^-)$
Band $\gamma \rightarrow$ Band 1										
682.0	2169.5	11(3)		1.3(6)					$(M1/E2)$	$23/2^- \rightarrow 23/2^-$
689.5	1559.8	15(5)							$(M1/E2)$	$19/2^- \rightarrow 19/2^-$
692.3	1089.9	11(5)							$(M1/E2)$	$15/2^- \rightarrow 15/2^-$
979.9	1089.9	35(25)		1.6(4)					$E2$	$15/2^- \rightarrow 11/2^-$
1163.4	1559.8	43(14)		1.5(5)					$E2$	$19/2^- \rightarrow 15/2^-$
1297.6	2169.5	9(2)		1.4(4)					$E2$	$23/2^- \rightarrow 19/2^-$
Band $\gamma \rightarrow$ Band 2										
531.0	2169.5	15(3)		1.4(5)					$E2$	$23/2^- \rightarrow 19/2^-$
Band 1										
286.7	396.9	1000	1.00(6)[e]				0.11(2)		$E2$	$15/2^- \rightarrow 11/2^-$
473.9	870.7	887(19)	1.00(9)[e]				0.12(4)		$E2$	$19/2^- \rightarrow 15/2^-$
542.6	939.5	33(10)							$(M1/E2)$	$(17/2^-) \rightarrow 15/2^-$
616.8	1487.5	623(25)	1.1(1)[e]				0.12(4)		$E2$	$23/2^- \rightarrow 19/2^-$
646.6	1586.1	18(7)							$(E2)$	$(21/2^-) \rightarrow (17/2^-)$
740.1	2326.2	13(6)							$(E2)$	$(25/2^-) \rightarrow (21/2^-)$
731.4	2218.9	425(30)	1.11(7)[e]				0.12(4)		$E2$	$27/2^- \rightarrow 23/2^-$
828.5	3047.4	290(15)	1.03(6)[e]				0.08(3)		$E2$	$31/2^- \rightarrow 27/2^-$
835.0	3161.2	11(6)							$(E2)$	$(29/2^-) \rightarrow (25/2^-)$
913.6	3961.0	106(8)	0.99(5)[e]				0.07(2)		$E2$	$35/2^- \rightarrow 31/2^-$
945.7	4106.9	10(6)							$(E2)$	$(33/2^-) \rightarrow (29/2^-)$
989.9	4950.9	44(4)	0.90(8)[e]				0.07(4)		$E2$	$39/2^- \rightarrow 35/2^-$
1055.2	6006.1	31(3)	1.0(2)[e]						$E2$	$43/2^- \rightarrow 39/2^-$
1124.5	7130.6	18(2)	1.0(4)[e]						$E2$	$47/2^- \rightarrow 43/2^-$
1194.7	8325.3	15(2)	1.0(4)[e]						$E2$	$51/2^- \rightarrow 47/2^-$
1266.5	9591.8	10(2)	1.0(4)[e]						$E2$	$55/2^- \rightarrow 51/2^-$
1333.7	10925.5	7(2)		1.5(3)					$E2$	$59/2^- \rightarrow 55/2^-$
1372.6	12298.1	4(1)		1.3(3)					$E2$	$63/2^- \rightarrow 59/2^-$
1401.0	13699.1	1(1)							$(E2)$	$(67/2^-) \rightarrow 63/2^-$
Band 1 $\rightarrow$ $7/2^+$ $\rightarrow$ Ground state										
(23.1)	110.2								$(M2)$	$11/2^- \rightarrow (7/2^+)$
87.1	87.1								$(E2)$	$(7/2^+) \rightarrow 3/2^+$
Band 1 $\rightarrow$ Band 8										
(24.5)	110.2								$(E1)$	$11/2^- \rightarrow 9/2^+$
Band 2										
310.0	2128.4	4(1)							$(M1/E2)$	$23/2^- \rightarrow 21/2^-$
373.4	1637.7	10(2)		1.1(4)					$(M1/E2)$	$19/2^- \rightarrow 17/2^-$
380.2	1637.7	19(4)	1.0(2)[e]	1.3(2)					$E2$	$19/2^- \rightarrow 15/2^-$
490.9	2128.4	48(3)	1.0(2)[e]				0.10(5)		$E2$	$23/2^- \rightarrow 19/2^-$

TABLE II. (*Continued.*)

E_γ (keV)[a]	E_i (keV)	I_γ^b	R_{DCO}^c	R_{ac}^d	a_2	a_4	A_P	δ	Mult.	$J_i^\pi \rightarrow J_f^\pi$
553.7	1818.1	13(3)	0.9(2)[e]						$E2$	$21/2^- \rightarrow 17/2^-$
577.3	2705.7	112(9)	1.0(1)[e]	1.5(2)			0.13(3)		$E2$	$27/2^- \rightarrow 23/2^-$
630.9	3336.8	150(15)	1.2(2)[e]				0.10(3)		$E2$	$31/2^- \rightarrow 27/2^-$
678.5	2496.7	27(4)	1.2(2)[e]				0.2(1)		$E2$	$25/2^- \rightarrow 21/2^-$
707.4	4044.9	8(3)		0.8(3)					$M1/E2$	$33/2^- \rightarrow 31/2^-$
728.1	4064.9	149(46)	0.9(1)[e]				0.11(5)		$E2$	$35/2^- \rightarrow 31/2^-$
764.0	3260.8	56(20)	1.1(3)[e]				0.19(8)		$E2$	$29/2^- \rightarrow 25/2^-$
766.4	4831.7	20(11)		0.9(3)					$M1/E2$	$37/2^- \rightarrow 35/2^-$
784.2	4044.9	20(10)	1.0(4)[e]						$E2$	$33/2^- \rightarrow 29/2^-$
787.2	4831.7	19(10)	1.0(4)[e]						$E2$	$37/2^- \rightarrow 33/2^-$
820.3	5714.1	7(4)							$(M1/E2)$	$41/2^- \rightarrow 39/2^-$
828.8	4893.7	114(14)	1.2(3)[e]				0.17(9)		$E2$	$39/2^- \rightarrow 35/2^-$
877.2	6699.5	4(2)							$(M1/E2)$	$45/2^- \rightarrow 43/2^-$
882.4	5714.1	13(6)	0.9(2)[e]						$E2$	$41/2^- \rightarrow 37/2^-$
929.3	5823.0	84(10)	1.2(4)[e]				0.18(11)		$E2$	$43/2^- \rightarrow 39/2^-$
985.1	6699.5	11(4)	1.0(3)[e]						$E2$	$45/2^- \rightarrow 41/2^-$
1026.1	6849.1	69(10)	1.1(3)[e]				0.09(5)		$E2$	$47/2^- \rightarrow 43/2^-$
1079.5	7779.0	10(4)	0.9(3)[e]						$E2$	$49/2^- \rightarrow 45/2^-$
1124.8	7973.9	43(10)	0.9(3)[e]						$E2$	$51/2^- \rightarrow 47/2^-$
1164.4	8943.4	8(4)	1.0(5)[e]						$E2$	$53/2^- \rightarrow 49/2^-$
1223.9	9197.8	33(8)	0.9(3)[e]						$E2$	$55/2^- \rightarrow 51/2^-$
1245.2	10188.6	5(3)		1.4(3)					$(E2)$	$(57/2^-) \rightarrow 53/2^-$
1311.0	10508.8	22(6)	1.0(3)[e]						$E2$	$59/2^- \rightarrow 55/2^-$
1345.0	11533.6	2.1(9)		1.5(6)					$(E2)$	$(61/2^-) \rightarrow 57/2^-$
1371.0	13256.2	3(2)		1.4(4)					$(E2)$	$(67/2^-) \rightarrow 63/2^-$
1376.4	11885.2	18(5)	1.0(3)[e]						$E2$	$63/2^- \rightarrow 59/2^-$
1389.1	13274.3	11(4)		1.3(3)					$(E2)$	$(67/2^-) \rightarrow (63/2^-)$
1405.8	12939.4	2(2)		1.5(6)					$(E2)$	$(65/2^-) \rightarrow (61/2^-)$
1455.5	14729.8	4(2)		1.4(4)					$(E2)$	$(71/2^-) \rightarrow (67/2^-)$
1474.5	14729.8	3(2)		1.5(5)					$(E2)$	$(71/2^-) \rightarrow (67/2^-)$
1543.7	16273.5	3(2)		1.4(5)					$(E2)$	$(75/2^-) \rightarrow (71/2^-)$
1674.7	17948.2	2(1)		1.3(6)					$(E2)$	$(79/2^-) \rightarrow (75/2^-)$
1857.4	19805.6	<2							$(E2)$	$(83/2^-) \rightarrow (79/2^-)$
Band 2 → Band γ										
568.8	2128.4	53(7)		1.3(2)					$E2$	$23/2^- \rightarrow 19/2^-$
Band 2 → (15/2$^-$)										
267.5	1637.7	7(5)							$(E2)$	$19/2^- \rightarrow (15/2^-)$
Band 2 → Band 1										
288.4	3336.8	6(3)							$(M1/E2)$	$31/2^- \rightarrow 31/2^-$
317.3	1257.8	4.2(10)							$(M1/E2)$	$15/2^- \rightarrow (17/2^-)$
393.4	1264.2	5(2)							$(M1/E2)$	$17/2^- \rightarrow 19/2^-$
486.6	2705.7	44(7)		1.4(2)					$M1/E2$	$27/2^- \rightarrow 27/2^-$
640.4	2128.4	35(5)		1.3(4)					$M1/E2$	$23/2^- \rightarrow 23/2^-$
766.7	1637.7	24(3)		1.4(4)					$M1/E2$	$19/2^- \rightarrow 19/2^-$
861.2	1257.8	15(1)		1.4(3)					$M1/E2$	$15/2^- \rightarrow 15/2^-$
867.8	1264.2	8(2)		0.8(3)					$M1/E2$	$17/2^- \rightarrow 15/2^-$
947.5	1818.1	47(10)		0.8(1)					$M1/E2$	$21/2^- \rightarrow 19/2^-$
998.5	4044.9	2(1)							$(M1/E2)$	$33/2^- \rightarrow 31/2^-$
1009.2	2496.7	39(13)		0.6(3)					$M1/E2$	$25/2^- \rightarrow 23/2^-$
1017.4	4064.9	20(8)		1.6(6)					$E2$	$35/2^- \rightarrow 31/2^-$
1042.0	3260.8	36(8)		0.7(5)					$M1/E2$	$29/2^- \rightarrow 27/2^-$
1118.5	3336.8	47(10)		1.6(4)					$E2$	$31/2^- \rightarrow 27/2^-$
1218.5	2705.7	55(10)		1.3(3)					$E2$	$27/2^- \rightarrow 23/2^-$
1241.2	1637.7	10(5)							$(E2)$	$19/2^- \rightarrow 15/2^-$
1258.0	2128.4	48(8)		1.3(5)					$(E2)$	$23/2^- \rightarrow 19/2^-$
(15/2$^-$) → Band 1										
498.9	1370.1	2(1)								$(15/2^-) \rightarrow 19/2^-$

TABLE II. (*Continued.*)

E_γ (keV)[a]	E_i (keV)	I_γ^b	R_{DCO}^c	R_{ac}^d	a_2	a_4	A_P	δ	Mult.	$J_i^\pi \rightarrow J_f^\pi$
973.4	1370.1	5(2)								$(15/2^-) \rightarrow 15/2^-$
Band 3										
279.6	949.4	68(4)	0.52(8)[e]				-0.09(3)		$M1/E2$	$(13/2^-) \rightarrow (11/2^-)$
315.2	1264.6	51(5)	1.2(2)[f]		-0.14(14)	0.08(27)	-0.06(2)	0.10(15)	$M1/E2$	$(15/2^-) \rightarrow (13/2^-)$
345.1	1609.8	40(5)	1.2(2)[f]		-0.06(11)	0.08(21)	-0.10(4)	0.10(10)	$M1/E2$	$(17/2^-) \rightarrow (15/2^-)$
370.1	1980.0	28(4)	1.1(2)[f]		0.01(16)	0.06(30)		0.15(15)	$M1/E2$	$(19/2^-) \rightarrow (17/2^-)$
389.9	2369.6	18(3)	1.0(2)[f]		-0.09(14)	0.21(27)	-0.06(4)	0.10(20)	$M1/E2$	$(21/2^-) \rightarrow (19/2^-)$
403.6	2773.6	15(2)	1.1(2)[f]		0.05(3)	0.11(6)		0.20(15)	$M1/E2$	$(23/2^-) \rightarrow (21/2^-)$
411.7	4011.9	8(2)		0.7(2)					$M1/E2$	$(29/2^-) \rightarrow (27/2^-)$
412.5	3185.8	5(2)		0.9(2)					$M1/E2$	$(25/2^-) \rightarrow (23/2^-)$
414.4	3600.8	5(3)		0.7(2)					$M1/E2$	$(27/2^-) \rightarrow (25/2^-)$
416.2	4428.3	5(3)		0.8(2)					$M1/E2$	$(31/2^-) \rightarrow (29/2^-)$
595.1	1264.6	7(2)		1.3(3)					$E2$	$(15/2^-) \rightarrow (11/2^-)$
660.6	1609.8	20(4)	1.9(5)[f]				0.08(4)		$E2$	$(17/2^-) \rightarrow (13/2^-)$
715.5	1980.0	24(4)	2.1(6)[f]				0.09(4)		$E2$	$(19/2^-) \rightarrow (15/2^-)$
759.5	2369.6	23(4)	2.2(3)[f]				0.09(4)		$E2$	$(21/2^-) \rightarrow (17/2^-)$
793.8	2773.6	25(4)	1.0(2)[e]				0.04(2)		$E2$	$(23/2^-) \rightarrow (19/2^-)$
816.2	3185.8	30(5)	0.9(2)[e]				0.07(5)		$E2$	$(25/2^-) \rightarrow (21/2^-)$
826.1	4011.9	22(15)	1.2(3)[e]						$E2$	$(29/2^-) \rightarrow (25/2^-)$
827.2	3600.8	28(17)		1.4(3)					$E2$	$(27/2^-) \rightarrow (23/2^-)$
827.5	4428.3	21(15)		1.4(3)					$E2$	$(31/2^-) \rightarrow (27/2^-)$
843.4	4855.3	16(3)	1.0(3)[e]						$E2$	$(33/2^-) \rightarrow (29/2^-)$
870.6	5298.9	16(4)	1.0(2)[e]						$E2$	$(35/2^-) \rightarrow (31/2^-)$
908.7	5764.0	10(2)	0.9(2)[e]						$E2$	$(37/2^-) \rightarrow (33/2^-)$
952.0	6250.9	13(4)	1.1(4)[e]						$E2$	$(39/2^-) \rightarrow (35/2^-)$
997.1	6761.0	7(2)	0.9(3)[e]						$E2$	$(41/2^-) \rightarrow (37/2^-)$
1042.1	7293.0	10(3)	1.1(5)[e]						$E2$	$(43/2^-) \rightarrow (39/2^-)$
1088.2	7849.3	7(2)	1.1(4)[e]						$E2$	$(45/2^-) \rightarrow (41/2^-)$
1132.2	8425.2	9(3)		1.4(4)					$E2$	$(47/2^-) \rightarrow (43/2^-)$
1176.9	9026.2	6(2)		1.3(3)					$(E2)$	$(49/2^-) \rightarrow (45/2^-)$
1218.6	9643.8	4(2)		1.3(4)					$(E2)$	$(51/2^-) \rightarrow (47/2^-)$
1258.8	10285.0	4(2)		1.5(4)					$(E2)$	$(53/2^-) \rightarrow (49/2^-)$
1299.7	10943.5	3(1)		1.3(3)					$(E2)$	$(55/2^-) \rightarrow (51/2^-)$
1340.4	11625.4	2.0(8)		1.5(5)					$(E2)$	$(57/2^-) \rightarrow (53/2^-)$
1377.4	12320.9	1.9(9)		1.2(4)					$(E2)$	$(59/2^-) \rightarrow (55/2^-)$
1416.5	13041.9	1.1(6)		1.3(5)					$(E2)$	$(61/2^-) \rightarrow (57/2^-)$
1454.3	13775.2	1.6(9)		1.4(7)					$(E2)$	$(63/2^-) \rightarrow (59/2^-)$
1492.0	14533.9	<1							$(E2)$	$(65/2^-) \rightarrow (61/2^-)$
1531.0	15306.2	<2							$(E2)$	$(67/2^-) \rightarrow (63/2^-)$
1574.0	16107.9	<1							$(E2)$	$(69/2^-) \rightarrow (65/2^-)$
Band 3→ Band populated by Band 3										
(26.4)	669.8								$(E1)$	$11/2^- \rightarrow 9/2^+$
294.2	669.8	2(1)							$(M2)$	$11/2^- \rightarrow 7/2^+$
Band populated by Band 3										
138.6	138.6	4(2)	0.8(2)[f]	0.72(8)					$M1/E2$	$5/2^+ \rightarrow 3/2^+$
237.0	375.6	5(1)	0.5(1)[e]	0.69(7)					$M1/E2$	$7/2^+ \rightarrow 5/2^+$
267.8	643.3	4(2)	0.9(2)[f]	1.0(2)					$M1/E2$	$9/2^+ \rightarrow 7/2^+$
Band 4										
331.8	475.9	19(5)	1.0(1)[e]						$E2$	$9/2^+ \rightarrow 5/2^+$
475.2	951.1	26(10)	1.1(1)[e]						$E2$	$13/2^+ \rightarrow 9/2^+$
541.0	1492.5	28(5)	0.9(2)[e]						$E2$	$17/2^+ \rightarrow 13/2^+$
562.3	2054.8	31(5)	1.0(1)[e]				0.11(4)		$E2$	$21/2^+ \rightarrow 17/2^+$
585.3	2640.1	36(6)	1.1(2)[e]				0.2(2)		$E2$	$25/2^+ \rightarrow 21/2^+$
636.3	3276.4	55(10)	1.0(1)[e]				0.04(2)		$E2$	$29/2^+ \rightarrow 25/2^+$
724.8	4001.2	47(9)	1.0(2)[e]				0.03(2)		$E2$	$33/2^+ \rightarrow 29/2^+$
826.1	4827.3	43(9)	0.9(2)[e]				0.2(1)		$E2$	$37/2^+ \rightarrow 33/2^+$
896.2	5723.5	31(7)	0.9(2)[e]						$E2$	$41/2^+ \rightarrow 37/2^+$
979.0	6702.5	18(5)	1.1(2)[e]						$E2$	$45/2^+ \rightarrow 41/2^+$
1064.5	7767.0	16(4)	0.8(2)[e]						$E2$	$49/2^+ \rightarrow 45/2^+$

TABLE II. (*Continued.*)

E_γ (keV)[a]	E_i (keV)	I_γ^b	R_{DCO}^c	R_{ac}^d	a_2	a_4	A_P	δ	Mult.	$J_i^\pi \rightarrow J_f^\pi$
1145.8	8912.8	15(4)	0.9(4)[e]						$(E2)$	$(53/2^+) \rightarrow 49/2^+$
1257.5	10170.3	10(4)	1.0(4)[e]						$(E2)$	$(57/2^+) \rightarrow (53/2^+)$
Band 4 → Band 1										
952.8	4001.2	4(2)							$(E1)$	$33/2^+ \rightarrow 31/2^-$
1058.1	3276.4	28(5)	0.5(2)[e]		-0.21(22)	0.25(47)	0.09(7)	0.00(25)	$E1$	$29/2^+ \rightarrow 27/2^-$
1095.6	1492.5	8.2(30)	0.6(1)[e]		-0.17(35)	0.19(67)	0.1(1)	0.05(25)	$(E1)$	$17/2^+ \rightarrow 15/2^-$
1152.5	2640.1	30(5)	0.5(1)[e]		-0.53(11)	0.16(22)	0.09(6)	-0.15(25)	$E1$	$25/2^+ \rightarrow 23/2^-$
1184.2	2054.8	22(3)	0.6(2)[e]		-0.28(20)	0.09(38)	0.1(1)	0.00(10)	$(E1)$	$21/2^+ \rightarrow 19/2^-$
Band 4 → Band 5										
267.2	475.9	7(2)		1.4(4)					$E2$	$9/2^+ \rightarrow 5/2^+$
328.0	951.1	3(2)							$(E2)$	$13/2^+ \rightarrow 9/2^+$
Band 4′										
1194.1	12545.8	5(3)		1.2(5)					$(E2)$	$(65/2^+) \rightarrow (61/2^+)$
1308.2	13854.0	3(2)		1.3(5)					$(E2)$	$(69/2^+) \rightarrow (65/2^+)$
1369.4	15223.4	3(2)		1.3(4)					$(E2)$	$(73/2^+) \rightarrow (69/2^+)$
1487.1	16710.5	2(1)		1.7(5)					$(E2)$	$(77/2^+) \rightarrow (73/2^+)$
1623.4	18333.9	<1							$(E2)$	$(81/2^+) \rightarrow (77/2^+)$
1768.3	20102.2	<1							$(E2)$	$(85/2^+) \rightarrow (81/2^+)$
Band 4′ → Band 4										
1181.4	11351.7	9(4)		1.2(6)					$(E2)$	$(61/2^+) \rightarrow (57/2^+)$
Band 5										
414.1	622.8	102(20)	0.9(1)[e]				0.08(2)		$E2$	$9/2^+ \rightarrow 5/2^+$
548.6	1171.4	88(30)	1.2(1)[e]				0.003(2)		$E2$	$13/2^+ \rightarrow 9/2^+$
594.0	1765.4	77(16)	1.0(2)[e]				0.06(4)		$E2$	$17/2^+ \rightarrow 13/2^+$
539.7	2305.1	65(9)	1.0(2)[e]				0.05(3)		$E2$	$21/2^+ \rightarrow 17/2^+$
590.1	2895.2	61(12)	1.00(8)[e]				0.00(1)		$E2$	$25/2^+ \rightarrow 21/2^+$
684.3	3579.5	40(7)	1.06(9)[e]						$E2$	$29/2^+ \rightarrow 25/2^+$
775.2	4354.7	29(4)	1.2(2)[e]						$E2$	$33/2^+ \rightarrow 29/2^+$
824.4	4403.9	3(2)		1.2(4)					$(E2)$	$(33/2^+) \rightarrow 29/2^+$
864.1	5218.8	20(5)	1.0(2)[e]						$E2$	$37/2^+ \rightarrow 33/2^+$
949.7	6168.5	14(4)	1.1(3)[e]						$E2$	$41/2^+ \rightarrow 37/2^+$
1032.3	7200.8	10(3)	1.0(3)[e]						$E2$	$45/2^+ \rightarrow 41/2^+$
1121.9	8322.7	5(2)		1.5(4)					$(E2)$	$(49/2^+) \rightarrow 45/2^+$
1202.5	9525.2	5(2)		1.3(3)					$(E2)$	$(53/2^+) \rightarrow (49/2^+)$
1287.3	10812.5	3(1)		1.4(6)					$(E2)$	$(57/2^+) \rightarrow (53/2^+)$
1367.3	12179.8	2(1)		1.4(7)					$(E2)$	$(61/2^+) \rightarrow (57/2^+)$
1443.3	13623.1	0.8(5)							$(E2)$	$(65/2^+) \rightarrow (61/2^+)$
1508.0	15131.1	0.8(5)							$(E2)$	$(69/2^+) \rightarrow (65/2^+)$
Band 5 → Ground state										
208.7	208.7	96(18)		0.80(9)	-0.29(4)	0.24(7)	-0.001(1)	0.10(20)	$M1/E2$	$5/2^+ \rightarrow 3/2^+$
Band 4 and Band 5 → $3/2^+$ or $1/2^+$ → Ground state										
(32.2)	144.1								$(E2)$	$5/2^+ \rightarrow (1/2^+)$
40.6	144.1	1.2(6)							$(M1/E2)$	$5/2^+ \rightarrow (3/2^+)$
96.2	208.7	0.7(3)							$(E2)$	$5/2^+ \rightarrow (1/2^+)$
102.8	102.8	12(6)	0.5(2)[e]	0.7(2)					$M1/E2$	$(3/2^+) \rightarrow 3/2^+$
105.1	208.7	7(3)						-	$(M1/E2)$	$5/2^+ \rightarrow (3/2^+)$
111.9	111.9	6(3)		0.8(2)					$M1/E2$	$(1/2^+) \rightarrow 3/2^+$
Band 5 → Band 4										
63.9	208.7	1(1)							$(M1/E2)$	$5/2^+ \rightarrow 5/2^+$
Band 5′										
598.0	2408.4	5(3)							$(E2)$	$(a21/2^+) \rightarrow 17/2^+$
678.6	3087.1	9(2)	1.1(4)[e]	1.3(3)					$E2$	$(25/2^+) \rightarrow (21/2^+)$
743.0	3830.1	6(2)		1.5(5)					$(E2)$	$(29/2^+) \rightarrow (25/2^+)$
766.9	4597.0	6(3)		1.4(5)					$(E2)$	$(33/2^+) \rightarrow (29/2^+)$
810.5	5407.5	3(1)		1.5(4)					$(E2)$	$(37/2^+) \rightarrow (33/2^+)$
906.3	6313.8	2(1)		1.5(7)					$(E2)$	$(41/2^+) \rightarrow (37/2^+)$
982.2	7296.0	2(1)		1.5(7)					$(E2)$	$(45/2^+) \rightarrow (41/2^+)$
Band 5′ → Band 5										
638.9	1810.3	5(3)		1.4(7)					$(E2)$	$(17/2^+) \rightarrow 13/2^+$
643.1	2408.4	4(3)		1.4(5)					$(E2)$	$(21/2^+) \rightarrow 17/2^+$

TABLE II. (*Continued.*)

E_γ (keV)[a]	E_i (keV)	I_γ^b	R_{DCO}^c	R_{ac}^d	a_2	a_4	A_P	δ	Mult.	$J_i^\pi \rightarrow J_f^\pi$
Band 6										
205.3	2583.9	11(5)		0.8(2)	-0.78(24)	0.14(44)	-0.13(13)	-0.35(25)	$M1/E2$	$(23/2^+) \rightarrow (21/2^+)$
207.5	3261.7	10(6)		0.7(2)					$M1/E2$	$(29/2^+) \rightarrow (27/2^+)$
208.9	2792.9	11(6)		0.8(2)					$M1/E2$	$(25/2^{+)} \rightarrow (23/2^+)$
238.9	3500.6	6(5)		0.8(1)					$M1/E2$	$(31/2^+) \rightarrow (29/2^+)$
261.3	3054.2	11(5)		0.8(1)					$M1/E2$	$(27/2^+) \rightarrow (25/2^+)$
311.2	3811.8	8(2)		0.8(2)					$M1/E2$	$(33/2^+) \rightarrow (31/2^+)$
415.0	2792.9	9(4)		1.4(4)					$E2$	$(25/2^+) \rightarrow (21/2^+)$
Band 6 $\rightarrow$ (21/2$^+$)										
164.3	2583.9	7(3)		0.8(1)					$M1/E2$	$(23/2^+) \rightarrow (21/2^+)$
(21/2$^+$) $\rightarrow$ Band 1 and Band 4										
926.0	2420.2	3(2)							$(E2)$	$(21/2^+) \rightarrow 17/2^+$
1549.5	2420.2	14(5)		0.9(2)			0.02(2)		$E1$	$(21/2^+) \rightarrow 19/2^-$
Band 6 $\rightarrow$ Band 1										
1508.0	2378.2	23(5)		0.8(2)			0.10(9)		$(E1)$	$(21/2^+) \rightarrow 19/2^-$
Band 6 $\rightarrow$ Band 4										
738.1	2792.9	10(5)		1.3(2)			0.13(12)		$E2$	$(25/2^+) \rightarrow 21/2^+$
886.5	2378.2	7(4)		1.4(4)					$E2$	$(21/2^+) \rightarrow 17/2^+$
926.0	2420.2	3(2)							$(E2)$	$(21/2^+) \rightarrow 17/2^+$
Band 6 $\rightarrow$ Band 8										
412.0	3811.8	25(6)		1.6(3)					$E2$	$(33/2^+) \rightarrow 29/2^+$
472.9	3500.6	14(10)		1.3(3)			0.06(6)		$E2$	$(31/2^+) \rightarrow 27/2^+$
Band 7										
744.8	4848.9	60(15)	1.1(1)[e]				0.05(2)		$E2$	$(37/2^+) \rightarrow (33/2^+)$
854.0	5702.8	59(12)	0.92(9)[e]						$E2$	$(41/2^+) \rightarrow (37/2^+)$
954.8	6657.6	47(10)	0.91(7)[e]				0.13(7)		$E2$	$(45/2^+) \rightarrow (41/2^+)$
1033.5	7691.1	28(6)	1.1(1)[e]				0.12(11)		$E2$	$(49/2^+) \rightarrow (45/2^+)$
1078.9	8770.0	21(5)	0.9(1)[e]						$E2$	$(53/2^+) \rightarrow (49/2^+)$
1150.6	9920.6	14(4)	0.9(2)[e]						$E2$	$(57/2^+) \rightarrow (53/2^+)$
1203.7	11124.3	11(4)	1.0(2)[e]						$E2$	$(61/2^+) \rightarrow (57/2^+)$
1272.6	12396.9	9(4)	0.9(4)[e]						$E2$	$(65/2^+) \rightarrow (61/2^+)$
1388.4	13785.3	7(4)	1.0(3)[e]						$E2$	$(69/2^+) \rightarrow (65/2^+)$
1522.5	15307.8	1.4(9)		1.3(3)					$E2$	$(73/2^+) \rightarrow (69/2^+)$
1672.7	16980.5	<1							$(E2)$	$((77/2^+) \rightarrow (73/2^+)$
1805.4	18785.9	<1							$(E2)$	$(81/2^+) \rightarrow (77/2^+)$
Band 7 $\rightarrow$ Band 6										
292.0	4104.0	19(5)		1.3(1)			-0.07(6)		$(M1/E2)$	$(33/2^+) \rightarrow (33/2^+)$
603.3	4104.0	23(6)	0.5(2)[e]						$M1/E2$	$(33/2^+) \rightarrow (31/2^+)$
Band 7 $\rightarrow$ Band 8										
704.4	4104.0	19(4)	1.1(3)[e]						$(E2)$	$(33/2^+) \rightarrow 29/2^+$
Band 8										
238.6	324.3	636(21)	1.02(5)[f]		-0.33(13)	0.18(25)	-0.04(1)	-0.05(30)	$M1/E2$	$11/2^+ \rightarrow 9/2^+$
268.6	592.9	530(12)	1.04(5)[f]		-0.32(14)	0.16(27)	-0.04(1)	-0.05(25)	$M1/E2$	$13/2^+ \rightarrow 11/2^+$
296.5	889.5	326(10)	1.06(5)[f]		-0.28(13)	0.19(25)	-0.02(1)	0.00(20)	$M1/E2$	$15/2^+ \rightarrow 13/2^+$
320.8	1210.4	230(8)	1.04(5)[f]		-0.26(14)	0.13(27)	-0.08(2)	0.10(25)	$M1/E2$	$17/2^+ \rightarrow 15/2^+$
341.9	1552.7	163(9)	1.06(6)[f]		-0.28(14)	0.08(26)	-0.07(2)	0.00(10)	$M1/E2$	$19/2^+ \rightarrow 17/2^+$
357.7	1910.5	113(8)	1.04(7)[f]		-0.20(17)	0.10(32)	-0.04(2)	-0.05(20)	$M1/E2$	$21/2^+ \rightarrow 19/2^+$
369.4	2279.6	75(13)		0.78(9)	-0.33(18)	0.09(35)	-0.03(3)	-0.05(20)	$M1/E2$	$23/2^+ \rightarrow 21/2^+$
371.9	3399.8	34(7)		0.81(9)			-0.04(3)		$M1/E2$	$29/2^+ \rightarrow 27/2^+$
373.7	2653.4	52(10)		0.90(8)			-0.01(1)		$M1/E2$	$25/2^+ \rightarrow 23/2^+$
375.0	3027.9	47(10)		0.88(8)					$M1/E2$	$27/2^+ \rightarrow 25/2^+$
391.6	4187.4	25(3)	0.9(2)[f]						$M1/E2$	$33/2^+ \rightarrow 31/2^+$
396.3	3796.1	22(5)	1.1(2)[f]						$M1/E2$	$31/2^+ \rightarrow 29/2^+$
417.2	4604.8	15(5)		0.7(2)					$M1/E2$	$35/2^+ \rightarrow 33/2^+$
507.4	592.9	109(5)	1.0(2)[e]				0.11(3)		$E2$	$13/2^+ \rightarrow 9/2^+$
565.2	889.5	150(7)	1.0(2)[e]				0.09(3)		$E2$	$15/2^+ \rightarrow 11/2^+$
617.8	1210.4	89(3)	0.8(2)[e]				0.13(4)		$E2$	$17/2^+ \rightarrow 13/2^+$
663.2	1552.7	126(3)	1.2(2)[e]				0.12(4)		$E2$	$19/2^+ \rightarrow 15/2^+$
700.3	1910.5	104(6)	1.0(2)[e]				0.14(5)		$E2$	$21/2^+ \rightarrow 17/2^+$
726.9	2279.6	72(9)	1.0(2)[e]				0.11(4)		$E2$	$23/2^+ \rightarrow 19/2^+$
743.0	2653.4	86(16)	1.0(2)[e]				0.15(7)		$E2$	$25/2^+ \rightarrow 21/2^+$
746.3	3399.8	83(16)	1.2(4)[e]				0.12(6)		$E2$	$29/2^+ \rightarrow 25/2^+$
748.3	3027.9	36(8)	0.8(3)[e]				0.09(7)		$E2$	$27/2^+ \rightarrow 23/2^+$
768.2	3796.1	27(5)	0.9(2)[e]						$E2$	$31/2^+ \rightarrow 27/2^+$

TABLE II. (*Continued.*)

E_γ (keV)[a]	E_i (keV)	I_γ^b	R_{DCO}^c	R_{ac}^d	a_2	a_4	A_P	δ	Mult.	$J_i^\pi \rightarrow J_f^\pi$
787.5	4187.4	48(8)	0.9(2)[e]						$E2$	$33/2^+ \rightarrow 29/2^+$
808.8	4604.8	23(4)		1.2(2)					$E2$	$35/2^+ \rightarrow 31/2^+$
830.0	5017.4	23(4)		1.4(2)					$E2$	$37/2^+ \rightarrow 33/2^+$
906.6	5511.4	30(6)		1.2(2)					$E2$	$39/2^+ \rightarrow 35/2^+$
921.8	5939.2	14(3)		1.2(2)					$E2$	$41/2^+ \rightarrow 37/2^+$
997.3	6508.7	17(4)		1.3(3)					$E2$	$43/2^+ \rightarrow 39/2^+$
1046.1	6985.3	8(2)		1.3(3)					$E2$	$45/2^+ \rightarrow 41/2^+$
1088.2	7596.9	15(6)		1.4(3)					$E2$	$47/2^+ \rightarrow 43/2^+$
1136.7	8122.0	5(2)		1.4(3)					$E2$	$49/2^+ \rightarrow 45/2^+$
1173.4	8770.3	11(3)		1.4(3)					$E2$	$51/2^+ \rightarrow 47/2^+$
1244.2	9366.2	1.8(8)		1.5(5)					$(E2)$	$(53/2^+) \rightarrow 49/2^+$
1286.3	10056.6	7(2)		1.3(5)					$(E2)$	$(55/2^+) \rightarrow 51/2^+$
1367.0	10733.2	1.9(8)		1.6(5)					$(E2)$	$(57/2^+) \rightarrow (53/2^+)$
1388.0	11444.6	5(2)		1.8(9)					$(E2)$	$(59/2^+) \rightarrow (55/2^+)$
1488.2	12221.4	0.6(3)							$(E2)$	$(61/2^+) \rightarrow (57/2^+)$
1508.7	12953.3	3(2)		1.7(9)					$(E2)$	$(63/2^+) \rightarrow (59/2^+)$
Band 9										
292.2	1436.3	9(2)		0.8(2)	-0.27(6)	-0.01(5).	-0.05(5)	0.40(10)	$M1/E2$	$15/2^+ \rightarrow 13/2^+$
302.6	1738.8	11(2)	1.0(2)[f]		-0.22(5)	0.01(9)	-0.03(3)	0.00(10)	$M1/E2$	$17/2^+ \rightarrow 15/2^+$
314.0	2053.5	11(2)	1.0(1)[f]		-0.27(3)	-0.10(6)	-0.05(3)	0.00(20)	$M1/E2$	$19/2^+ \rightarrow 17/2^+$
327.0	2380.0	7(2)	1.1(3)[f]		-0.23(6).	-0.09(12)	-0.05(4)	0.00(10)	$M1/E2$	$21/2^+ \rightarrow 19/2^+$
340.9	2720.3	5(2)							$(M1/E2)$	$(23/2^+) \rightarrow 21/2^+$
341.5	3406.2	3(1)							$(M1/E2)$	$(27/2^+) \rightarrow (25/2^+)$
344.4	3065.0	5(2)							$(M1/E2)$	$(25/2^+) \rightarrow (23/2^+)$
344.8	3751.6	1.3(8)							$(M1/E2)$	$(29/2^+) \rightarrow (27/2^+)$
359.1	4109.8	<1							$(M1/E2)$	$(31/2^+) \rightarrow (29/2^+)$
376.3	4486.0	<1							$(M1/E2)$	$(33/2^+) \rightarrow (31/2^+)$
393.5	4880.3	<1							$(M1/E2)$	$(35/2^+) \rightarrow (33/2^+)$
421.1	5301.1	<1							$(M1/E2)$	$(37/2^+) \rightarrow (35/2^+)$
439.1	5740.7	<1							$(M1/E2)$	$(39/2^+) \rightarrow (37/2^+)$
616.3	2052.5	8(3)		1.4(5)					$(E2)$	$19/2^+ \rightarrow 15/2^+$
641.6	2380.0	6(2)		1.3(6)					$(E2)$	$21/2^+ \rightarrow 17/2^+$
667.1	2720.3	6(2)		1.4(5)					$(E2)$	$(23/2^+) \rightarrow 19/2^+$
685.3	3065.0	4(2)		1.5(9)					$(E2)$	$(25/2^+) \rightarrow 21/2^+$
685.6	3406.2	6(3)		1.5(9)					$(E2)$	$(27/2^+) \rightarrow (23/2^+)$
687.2	3751.6	3(2)		1.5(9)					$(E2)$	$(29/2^+) \rightarrow (25/2^+)$
702.7	4109.8	<6							$(E2)$	$(31/2^+) \rightarrow (27/2^+)$
734.2	4486.0	<3							$(E2)$	$(33/2^+) \rightarrow (29/2^+)$
771.3	4880.3	<6							$(E2)$	$(35/2^+) \rightarrow (31/2^+)$
814.8	5301.1	<3							$(E2)$	$(37/2^+) \rightarrow (33/2^+)$
860.4	5740.7	<6							$(E2)$	$(39/2^+) \rightarrow (35/2^+)$
Band 9 → Band 8										
819.5	1144.2	4(2)							$(M1/E2)$	$13/2^+ \rightarrow 11/2^+$
826.8	2380.0	4(2)							$(M1/E2)$	$21/2^+ \rightarrow 19/2^+$
841.5	2052.5	5(3)		0.7(5)					$M1/E2$	$19/2^+ \rightarrow 17/2^+$
843.5	1436.3	11(2)		0.9(2)					$M1/E2$	$15/2^+ \rightarrow 13/2^+$
849.1	1738.8	10(3)		1.0(5)					$(M1/E2)$	$17/2^+ \rightarrow 15/2^+$
1058.9	1144.2	5(2)							$(E2)$	$13/2^+ \rightarrow 9/2^+$
1111.9	1436.3	7(4)							$(E2)$	$15/2^+ \rightarrow 11/2^+$
Band 10										
174.4	1856.0	9(2)	0.9(4)[f]	0.7(2)			-0.02(1)		$M1/E2$	$19/2^+ \rightarrow 17/2^+$
207.1	2063.0	9(2)	1.0(3)[f]		-0.12(3)	0.02(4)	-0.01(1)	0.10(10)	$M1/E2$	$21/2^+ \rightarrow 19/2^+$
238.9	2302.2	12(4)		0.8(3)			-0.08(5)		$M1/E2$	$23/2^+ \rightarrow 21/2^+$
268.0	1681.3	<11		1.0(4)					$(M1/E2)$	$17/2^+ \rightarrow 15/2^+$
299.8	2602.0	10(2)	0.9(3)[f]		-0.53(52)	-0.24(96)	-0.05(4)	-0.15(40)	$M1/E2$	$25/2^+ \rightarrow 23/2^+$
332.7	2934.9	5.3(8)	1.0(3)[f]		-0.23(8)	-0.09(16)	-0.10(5)	0.00(10)	$M1/E2$	$27/2^+ \rightarrow 25/2^+$
359.9	3294.9	3.3(8)	1.0(2)[f]				-0.16(14)		$M1/E2$	$29/2^+ \rightarrow 27/2^+$
382.3	2063.0	1.9(7)							$(E2)$	$21/2^+ \rightarrow 17/2^+$
394.3	3690.1	3.3(9)							$(M1/E2)$	$31/2^+ \rightarrow 29/2^+$
420.8	4111.1	5(2)		0.7(2)					$M1/E2$	$33/2^+ \rightarrow 31/2^+$

TABLE II. (*Continued.*)

E_γ (keV)[a]	E_i (keV)	I_γ^b	R_{DCO}^c	R_{ac}^d	a_2	a_4	A_P	δ	Mult.	$J_i^\pi \rightarrow J_f^\pi$
446.8	2302.2	6.4(6)	1.0(2)[e]	1.4(4)					$E2$	$23/2^+ \rightarrow 19/2^+$
449.0	4560.8	1.9(9)							$(M1/E2)$	$35/2^+ \rightarrow 33/2^+$
632.8	2934.9	5.6(8)	0.9(2)[e]	1.3(4)					$E2$	$27/2^+ \rightarrow 23/2^+$
693.0	3294.9	3.0(6)		1.2(4)					$(E2)$	$29/2^+ \rightarrow 25/2^+$
755.2	3690.1	10(2)	1.1(3)[e]						$E2$	$31/2^+ \rightarrow 27/2^+$
816.2	4111.1	2.3(7)							$(E2)$	$33/2^+ \rightarrow 29/2^+$
870.7	4560.8	7(3)		1.4(5)					$(E2)$	$(35/2^+) \rightarrow 31/2^+$
925.2	5036.3	5(2)		1.4(4)					$(E2)$	$(37/2^+) \rightarrow 33/2^+$
975.5	5536.3	6(2)		1.3(4)					$(E2)$	$(39/2^+) \rightarrow (35/2^+)$
1012.0	6048.3	3(2)							$(E2)$	$(41/2^+) \rightarrow (37/2^+)$
1047.0	6583.3	4(2)							$(E2)$	$(43/2^+) \rightarrow (39/2^+)$
Band 10 → Band 8										
511.0	2063.0	1.3(8)							$(M1/E2)$	$21/2^+ \rightarrow 19/2^+$
646.2	1856.0	2.3(8)							$(M1/E2)$	$19/2^+ \rightarrow 17/2^+$
750.0	2302.2	<1							$E2$	$23/2^+ \rightarrow 19/2^+$
791.6	1681.3	2.9(6)							$(M1/E2)$	$17/2^+ \rightarrow 15/2^+$
852.7	2063.0	7.7(9)							$(E2)$	$21/2^+ \rightarrow 17/2^+$
966.6	1856.0	24(3)	1.9(7)[f]	1.3(3)			0.05(3)		$(E2)$	$19/2^+ \rightarrow 15/2^+$
1088.4	1413.6	<15							$(E2)$	$15/2^+ \rightarrow 11/2^+$
1088.4	1681.3	12(5)		1.4(3)					$E2$	$17/2^+ \rightarrow 13/2^+$

[a]The error on the transition energies is 0.3 keV for transitions below 500 keV, 0.7 keV for transitions between 500 and 1000 keV, and 1.0 keV for transitions above 1000 keV. The error on the transition energies is 1.0 keV for transitions with intensity less than 5.

[b]Relative intensities corrected for efficiency, normalized to the intensity of the 286.7 keV ($15/2^- \rightarrow 11/2^-$ of Band 1) transition [7]. The transition intensities were obtained from a combination of those measured for the total projection and gated spectra.

[c]R_{DCO} has been deduced from an asymmetric $\gamma - \gamma$ coincidence matrix sorted with the detectors at 157.6° on one axis, and detectors at $\approx 90°$ on the other axis. The tentative spin-parity of the states are given in parentheses.

[d]R_{ac} has been deduced from two asymmetric $\gamma - \gamma$ coincidence matrices sorted, respectively, with the detectors at 133.6° and 157.6° on one axis, and detectors at 75.5° and 104.5° on the other axis. The tentative spin-parity of the states are given in parentheses.

[e] DCO ratio from spectrum gated on stretched quadrupole transition.

[f] DCO ratio from spectrum gated on stretched dipole transition.